"© 2021 IEEE. Personal use of this material is permitted. Permission from IEEE must be obtained for all other uses, in any current or future media, including reprinting/republishing this material for advertising or promotional purposes, creating new collective works, for resale or redistribution to servers or lists, or reuse of any copyrighted component of this work in other works."

Cramér-Rao bounds and optimal design metrics for pose-graph SLAM

Yongbo Chen, Shoudong Huang, Liang Zhao, and Gamini Dissanayake

***Abstract*—2D/3D pose-graph simultaneous localization and mapping (SLAM) is a problem of estimating a set of poses based on noisy measurements of relative rotations and translations. This paper focuses on the relation between the graphical structure of pose-graph SLAM and Fisher information matrix (FIM), Cramér-Rao lower bounds (CRLB), and its optimal design metrics (T-optimality and D-optimality). As a main contribution, based on the assumption of isotropic Langevin noise for rotation and block-isotropic Gaussian noise for translation, the FIM and CRLB are derived and shown to be closely related to the graph structure, in particular, the weighted Laplacian matrix. We also prove that total node degree and weighted number of spanning trees, as two graph connectivity metrics, are respectively closely related to the trace and determinant of the FIM. The discussions show that, compared with the D-optimality metric, the T-optimality metric is more easily computed but less effective. We also present upper and lower bounds for the D-optimality metric, which can be efficiently computed and are almost independent of the estimation results. The results are verified with several well-known datasets, such as Intel, KITTI, sphere and so on.**

***Index Terms*—Pose-graph SLAM, Fisher information matrix (FIM), weighted Laplacian matrix, Cramér-Rao lower bounds (CRLB), optimal design metrics**

I. Introduction

SYNCHRONIZATION on the group of rigid body motions in two-dimensional (2D) plane and three-dimensional (3D) space, $\mathbb{R}^2 \times SO(2)$ and $\mathbb{R}^3 \times SO(3)$, is to estimate a set of poses based on noisy measurements of relative rotations and translations [1]. Multiple estimation problems, including pose-graph SLAM, fall into this category [2]. These synchronization problems in general give rise to a weighted graph representation. In essence, there is a correlation between the graphical structure of the 2D/3D pose-graph SLAM problem and its corresponding measurement network.

Given a pose-graph SLAM problem, assuming we can obtain its optimal solution using graph-based optimization method, one question to ask is how *reliable* that solution will be (i.e., accuracy compared to ground-truth and the uncertainty of the estimated solution). Both the covariance matrix and the FIM can be used to assess the uncertainty of the estimated parameters. However, compared with the FIM, updating/storing the dense full covariance matrix is prohibitively expensive with the growth of the dimension of the state vector. Thus, the FIM is the top-priority choice to evaluate the uncertainty of the SLAM solution in the maximum likelihood (ML) estimate. Under the assumption that the rotation noises obeying the isotropic Langevin distribution and using the Frobenius norm based distance, the state-of-the-art algorithms of SLAM, including SE-Sync [3] and Cartan-Sync [4], show outstanding computational efficiency (more than an order of magnitude faster) compared with the Gauss-Newton (GN) based approach. Nevertheless, the corresponding FIM is not presented in the literature.

From the graphical point of view, we know that adding relative measurements among the poses, which is equivalent to introducing new edges to the corresponding graph, helps to reduce the uncertainty of the estimator. In 2D pose-graph SLAM, the FIM has been proved to be closely related to the graph structure of the measurements network, in particular, the weighted Laplacian matrix [5] [6] assuming Gaussian noise on the relative pose orientation and ignoring the wraparound issue. In this paper, as the first contribution, we derive the FIM based on the assumption of zero-mean isotropic Langevin noise for orientation and block-isotropic Guassian noise for translation in 2D and 3D pose-graph SLAM.

It is known that, in a flat Euclidean space, the classical CRLB result for any unbiased estimator provides us with a simple but strong relation between the covariance matrix $\boldsymbol{C}$ and the FIM $\boldsymbol{F}$: $\boldsymbol{C} \succeq \boldsymbol{F}^{-1}$ [7]. Because of the non-flat property of the parameter space of 3D pose-graph SLAM, its CRLB does not follow this expression. The curvature terms of the space need to be considered to derive the rigorous CRLB. In this paper, we derive the CRLB for 2D and 3D pose-graph SLAM.

Because of the sparseness advantage of the FIM, the Theory of Optimal Experimental Design (TOED), including A-optimality, D-optimality, E-optimality, and T-optimality, on the FIM are widely used in decision making under uncertainty and belief space planning with applications including autonomous driving, surveillance and active SLAM [2]. For example, in [8], the D-optimality, E-optimality, and T-optimality metrics are used in active visual object reconstruction, and the T-optimality metric is applied to solve the sensor selection problem in Large Sensor Networks [9] [10]. The TOED is closely related to the graphical structure of the block design [11]. In 2D pose/feature-graph SLAM with the block-isotropic Gaussian noise, the D-optimality metric can be bounded by an expression related to the weighted number of spanning trees

Manuscript received January 22, 2020; accepted May 21, 2020. This article was recommended for publication by Associate Editor and Editor Chaumette, Francois upon evaluation of the reviewers' comments. (Corresponding author: Yongbo Chen.)

Yongbo Chen, Shoudong Huang, Liang Zhao, and Gamini Dissanayake are with Centre for Autonomous Systems, Faculty of Engineering and Information Technology, University of Technology, Sydney, Ultimo, NSW 2007, Australia (e-mail: Yongbo.Chen@student.uts.edu.au, Shoudong.Huang@uts.edu.au, Liang.Zhao@uts.edu.au, Gamini.Dissanayake@uts.edu.au).

Color versions of one or more of the figures in this article are available online at https://ieeexplore.ieee.org.

Digital Object Identifier 10.1109/TRO.2020.

[6]. In this paper, we extend the results in [6] into 3D pose-graph SLAM and also make a comparison between the T-optimality metric and the D-optimality metric from the point of view of the graphical structure of the measurement network.

A. Contributions

The main contributions of this paper are listed below.

- Extension of the formula derivation of the FIM and the CRLB of the synchronization problem in [12] from the rotation group $SO(n)$ to the group of rigid body motions, $\mathbb{R}^2 \times SO(2)$ and $\mathbb{R}^3 \times SO(3)$, based on the assumption of isotropic Lagevin noise (for rotation) and block-isotropic Guassian noise (for translation);
- Derivation of the relationship between the FIM of 3D pose-graph SLAM and the weighted Laplacian matrix;
- Extension of the analysis results of the D-optimality metric in [5] and [6] from 2D pose-graph SLAM into 3D case with $\mathbb{R}^3 \times SO(3)$ relative-pose measurements;
- Comparison of the D-optimality and T-optimality metrics of pose-graph SLAM from the graphical perspective.

B. Outline

In Section II, we review the related works about the pose-graph SLAM, the FIM, the CRLB and the TOED. In Section III, we provide a mathematical formulation of the synchronization on the group of rigid body motions in 2D plane and 3D space, $\mathbb{R}^n \times SO(n),\ n = 2, 3$. In Section IV, we present the FIM for 2D pose-graph SLAM and show its strong relationship with the weighted Laplacian matrix of the measurement graph. Furthermore, we obtain the FIM for the 3D situation and extend the relationship with the weighted Laplacian matrix into the $\mathbb{R}^3 \times SO(3)$ situation in Section V. In Section VI, the CRLB of 2D and 3D pose-graph SLAM are presented. The TOED metrics of the FIM of pose-graph SLAM are discussed focusing on the graph topology in Section VII. Simulation and experimental results are given in Section VIII. Conclusions, potential applications and future work are presented in Section IX.

C. Notations

Throughout this paper, unless otherwise noted, bold lowercase and bold uppercase letters are reserved for vectors and matrices, respectively. Sets are shown by uppercase letters. $\boldsymbol{S}_1 \succeq \boldsymbol{S}_2$ means matrix $\boldsymbol{S}_1 - \boldsymbol{S}_2$ is positive semidefinite. The Kronecker product is denoted by $\otimes$. trace$(\star)$ and $\det(\star)$ represent the trace and determinant of the matrix $\star$. We denote by diag$(\boldsymbol{M}_1, ..., \boldsymbol{M}_k)$ the block-diagonal matrix with matrices $\boldsymbol{M}_1, ..., \boldsymbol{M}_k$ as blocks on its main diagonal. The squared Frobenius norm is $\| \star \|_F^2 = \text{trace}(\star^\top \cdot \star)$. $\| \star \|_{eig}$ means the biggest eigenvalue of the matrix $\star$; For a symmetric positive definite matrix $\star$, $\| \star \|_{eig} = \| \star \|_2$. $SO(n)$ (special orthogonal group) and $\bar{O}(n)$ (orthogonal group) are respectively defined as: $SO(n) \triangleq \{\boldsymbol{R} \in \mathbb{R}^{n\times n} : \boldsymbol{R}^\top \boldsymbol{R} = \boldsymbol{I}_{n\times n},\ \det(\boldsymbol{R}) = 1\}$ and $\bar{O}(n) \triangleq \{\boldsymbol{G} \in \mathbb{R}^{n\times n} : \boldsymbol{G}^\top \boldsymbol{G} = \boldsymbol{I}_{n\times n}\}$. dist$(\star, \bullet) = \| \log(\star^\top \cdot \bullet) \|_F$ is the geodesic distance between $\star$ and $\bullet$ in $SO(n)$. The squared vector norm is $\| \star \|_2^2 = \star^\top \cdot \star$, for a vector $\star$. $|\star|$ means the cardinality of the set $\star$. $\mathbb{E}\{\star\}$ means the mathematical expectation of $\star$. $\nabla_\star \bullet$ means the partial derivative of a function $\bullet$ with respect to parameter $\star$. $\star \ltimes \bullet$ and $\star \times \bullet$ respectively mean the semi-product group and the direct product group of the group $\star$ and the group $\bullet$. ddiag$(\star)$ sets all off-diagonal entries of a square matrix $\star$ to zero.

II. Related work

Pose-graph SLAM leads to a non-convex optimization problem, whose (globally optimal) solution is the ML estimate for the unknown poses. It is well-known that SLAM back-end methods roughly fall into two categories. The first one is to use high-efficiency iterative nonlinear optimization methods based on GN method, Levenberg-Marquardt (LM) method and Powell's dogleg method, such as: g2o [13], iSAM2 [14], SLAM++ [15] and ceres [16], to obtain locally optimal solutions. Because of its non-convex property, starting from a poor initial guess, the iterative techniques may be trapped into a local minimum, which corresponds to a wrong estimate. The other one is to compute globally optimal solutions via convex relaxations [3] [17] [18]. Some works have shown that the duality gap of the general pose-graph SLAM problem in practical applications is close to zero [19], which implies that it can be solved exactly via convex relaxations. Beside pose-graph SLAM, the similar technologies have been widely used in other robotics and computer vision applications, such as: 3D registration [20] and structure from motion (SfM) [21].

Although many efficient optimization algorithms have been developed, the achievable estimated uncertainty is not well studied. Boumal [1] proposes the FIM for the estimation problems when the actual parameter space is a Riemannian submanifolds or a Riemannian quotient manifold. In [1], Boumal also shows two simple examples based on isotropic Gaussian noise: synchronization on the group of translation $\mathbb{R}^n$ and synchronization on the group of rotation $SO(3)$. In his later work [12], the conclusions are extended to the general rotation group $SO(n)$ based on several kinds of Gaussian-like, but non-Gaussian, noises, especially for the isotropic Langevin noise, which has attracted some robotics researchers' attention. As the state-of-the-art back-end algorithms, the convex relaxation based SE-Sync [3] and Cartan-Sync methods [4] are built based on the assumption of isotropic Gaussian noise (for translation) and isotropic Langevin noise (for rotation). To the best of our knowledge, the FIM for pose-graph SLAM based on these noises, whose parameter space is the product manifold $\mathbb{R}^n \times SO(n),\ n = 2, 3$, has not been analyzed.

CRLB, as a classical tool in estimation theory [22], provides a lower bound on the variance of any unbiased estimator for an estimated problem [12]. The traditional CRLB is defined in a flat Euclidean space. Smith [23] extends the theory of CRLB into the general non-flat manifold. Because the inverse of the FIM will become singular when no anchor is provided in the estimation problem, Xavier and Barroso [24] use the pseudoinverse of the FIM for the anchor-free case. Based on these new extended tools, Boumal presents the CRLB for the synchronization of rotations $SO(n)$ in both the anchored and the anchor-free cases. Pose-graph SLAM

is an anchored estimation problem in a product manifold $\mathbb{R}^n \times SO(n),\ n = 2, 3$ commonly. As an extension of [12], we will present its CRLB in this paper.

In fact, there are two different Lie group representations corresponding to 2D/3D pose-graph SLAM: $\mathbb{R}^n \times SO(n)$ and $SE(n) = \mathbb{R}^n \ltimes SO(n)$. The direct product of $SO(n)$ and $\mathbb{R}^n$ manifolds $\mathbb{R}^n \times SO(n)$ can be represented as a $(2n+1) \times (2n+1)$ matrix with $n + \frac{n(n-1)}{2}$-dimensional minimal representation. The $\mathbb{R}^n$ and $SO(n)$ group can be considered as two separated parts easily, because of the separated Riemannian structure (decided by inner product) [25]. The special Euclidean group $SE(n)$ is isomorphic to $\mathbb{R}^n \times SO(n)$, but with different Riemannian structure (semi-product) [26]. It can be represented as a $(n+1) \times (n+1)$ homogeneous transformation matrix with $n + \frac{n(n-1)}{2}$-dimensional minimal representation. Because of the different Riemannian structure, these two groups have the different tangent spaces and gradient forms, which leads to different FIM and CRLB. Compared with $SE(3)$, the direct product group $\mathbb{R}^n \times SO(n)$ can keep the bi-invariance property by the simple combined Riemannian metric, which is defined as the sum of the metrics of $\mathbb{R}^n$ and $SO(n)$. However, the manifold $SE(3)$ does not have any bi-invariant metric, which results in more complicated formulations for FIM, CRLB and curvature terms. Meanwhile, many recent popular SLAM pose-graph optimization methods, such as SE-sync method and initialization techniques [27], separate the problem into two parts: the rotation estimation and the linear least squares estimation for translation. Their objective functions are built based on the direct product group $\mathbb{R}^n \times SO(n)$. Hence, in this paper, we only consider the SLAM problem defined on the direct product group $\mathbb{R}^n \times SO(n)$.

For the TOED, a comparison of these optimality criteria is presented in [28] [29] [30]. In recent work, the authors show that the monotonicity of all optimality criteria (A-optimality, D-optimality, and E-optimality) and Shannons entropy is greatly affected by the uncertainty representation [31]. As a common representation, the uncertainty representations on the Lie group $SE(3)$ based on the Gaussian noise have also been considered [32]. In these metrics, the D-optimality metric and T-optimality metric do not need to perform the inverse operation for the FIM, which leads to a lower computational complexity. The D-optimality metric is the most popular metric with a good performance [28]. However, from the computational complexity perspective, the T-optimality metric still has its obvious advantage compared with the D-optimality metric, even though the state-of-the-art incremental technology could be used for computing the D-optimality metric [33]. So both metrics have great significance to the different estimation and planning requirements. We will investigate both two metrics based on the graphical structure of the SLAM.

In the previous work [5] [6] and [34], the authors analyze the impact of the graphical structure on some of the desirable attributes of some estimation problems: linear sensor network (SN), compass-SLAM and 2D pose-graph SLAM with block-isotropic Gaussian noise. In linear-SN and compass-SLAM, the FIM is proportional to the reduced Laplacian matrix of the corresponding graph, which helps to directly connect the optimal design of the FIM with the structure of the measurement graph. For 2D pose-graph SLAM with the block-isotropic Gaussian noises, it is stated that the D-optimality metric of the FIM can be bounded by an expression related to the weighted number of spanning trees of the measurement graph (weighted tree-connectivity). Based on the lower bounds, a new near-t-optimal graph synthesis framework is put forward for the measurement selection, pose-graph pruning problems and D-optimality-aware SLAM front-end. In this paper, we extend the conclusions [5], [6], [34] into 2D and 3D pose-SLAM with $\mathbb{R}^n \times SO(n),\ n = 2, 3$ relative-pose measurements.

III. Synchronization on $\mathbb{R}^n \times SO(n)$ (pose-graph SLAM)

In this section, we will present several concepts about the pose-graph SLAM, including the graph preliminaries, the problem formulation, the geometry of the parameter spaces and the definition of the FIM.

A. Graph preliminaries for pose-graph SLAM

A directed graph $\mathcal{G} = (\mathcal{V}, \mathcal{E})$, which is weakly connected, is used to represent pose-graph SLAM problem naturally. In this paper, $\mathcal{V} = \{0, 1, \cdots, n_p\}$, $\mathcal{E} \subseteq \mathcal{V} \times \mathcal{V}$ and $|\mathcal{E}| = m$. Each node corresponds to a robot pose, and each edge $(i, j) \in \mathcal{E}$ corresponds to a relative measurement from i-th robot pose to j-th robot pose. A new undirected rotation graph $\mathcal{G}_1 = (\mathcal{V}_1, \mathcal{F})$, whose nodes only represent the rotations of the poses and edges mean the relative rotation measurements, is created. It satisfies that $(i, j) \in \mathcal{F} \Rightarrow i \neq j$ and $(j, i) \in \mathcal{F}$. The rotation graph $\mathcal{G}_1$ is un-directed, because the relative rotation measurements (i, j) introduce the same information for i-th node and j-th node.

For the i-th node, we can define three node sets V_i^+, V_i^- and V_i satisfying $(i, j) \in \mathcal{E} \Leftrightarrow j \in V_i^+$, $(j, i) \in \mathcal{E} \Leftrightarrow j \in V_i^-$ and $V_i = V_i^- \bigcup V_i^+$, so we have $|V_i^+| + |V_i^-| = |V_i| = d_i$, where d_i is the node degree of the i-th node. Without loss of generality, the first pose (corresponding to 0-th node) is assumed to be the origin of our global coordinates system.

The incidence matrix of $\mathcal{G}$ is denoted by $\boldsymbol{A}_0 \in \{-1, 0, 1\}^{(n_p+1)\times m}$. $a_{ik} = -1$ and $a_{jk} = 1$ (the (i,k)-th and (j,k)-th elements of $\boldsymbol{A}_0$, k means the k-th measurement (edge)) are non-zero, if the k-th edge is $e_k = (i, j) \in \mathcal{E}$. The incidence matrix after anchoring to the origin, $\boldsymbol{A} \in \{-1, 0, 1\}^{n_p \times m}$, is obtained simply by removing the row corresponding to the first node in $\boldsymbol{A}_0$. The Laplacian matrix and the reduced Laplacian matrix of $\mathcal{G}$ are respectively defined as $\boldsymbol{L}_0 \triangleq \boldsymbol{A}_0 \boldsymbol{A}_0^\top$ and $\boldsymbol{L} \triangleq \boldsymbol{A}\boldsymbol{A}^\top$. It can be shown that $\boldsymbol{L}_0$ and $\boldsymbol{L}$ are respectively positive semi-definite and positive definite, if $\mathcal{G}$ is (weakly) connected. The Laplacian matrix and the reduced Laplacian matrix of $\mathcal{G}$ can be written as $\boldsymbol{L}_0 = \boldsymbol{D}_0 - \boldsymbol{W}_0$ and $\boldsymbol{L} = \boldsymbol{D} - \boldsymbol{W}$, where $\boldsymbol{D}_0 \triangleq \mathrm{diag}(d_0, d_1, \ldots, d_{n_p})$, $\boldsymbol{D} \triangleq \mathrm{diag}(d_1, \ldots, d_{n_p})$, $\boldsymbol{W}_0$ and $\boldsymbol{W}$ are respectively the original adjacency matrix and the adjacency matrix after removing the rows and columns corresponding to node 0. The weighted Laplacian matrix and the weighted reduced Laplacian matrix are defined as $\boldsymbol{L}_\omega^0 \triangleq \boldsymbol{A}_0 \boldsymbol{\Sigma}_0 \boldsymbol{A}_0^\top$ and $\boldsymbol{L}_\omega \triangleq \boldsymbol{A}\boldsymbol{\Sigma}\boldsymbol{A}^\top$, where $\boldsymbol{\Sigma}_0$ and $\boldsymbol{\Sigma}$ are diagonal matrices whose diagonal elements are the weight values of the graph edges.

B. Synchronization on $\mathbb{R}^n \times SO(n)$

Synchronization on the group of the rigid body motions in 2D plane and 3D space, $\mathbb{R}^n \times SO(n),\ n = 2, 3$, is the problem of estimating a set of positions $\boldsymbol{x}_0,\ \boldsymbol{x}_1, \cdots,\ \boldsymbol{x}_{n_p} \in \mathbb{R}^n$ and rotations $\boldsymbol{R}_0,\ \boldsymbol{R}_1, \cdots,\ \boldsymbol{R}_{n_p} \in SO(n)$ from noisy measurements of some relative rotations $\boldsymbol{R}_j\boldsymbol{R}_i^\top$ and relative coordinate transformations $\boldsymbol{R}_i^\top(\boldsymbol{x}_j - \boldsymbol{x}_i)$.

In 2D/3D pose-graph SLAM, including the anchored pose, the parameter space is: $\mathcal{P} = \{\mathbb{R}^n \times \cdots \times \mathbb{R}^n\}_{n_p+1} \times \{SO(n) \times \cdots \times SO(n)\}_{n_p+1}$.

For the pose-graph edge, $(i, j) \in \mathcal{E}$, we have the noisy measurement $\boldsymbol{p}_{ij} \in \mathbb{R}^n$ of the relative translation measurement between i-th and j-th poses:

$$\boldsymbol{p}_{ij} = \boldsymbol{R}_i^\top(\boldsymbol{x}_j - \boldsymbol{x}_i) + \boldsymbol{y}_{ij}, \tag{1}$$

where $\boldsymbol{y}_{ij} \sim \mathcal{N}(\boldsymbol{0}, \boldsymbol{\Sigma}_{ij})$, meaning that $\boldsymbol{y}_{ij}$ is a random vector, follows a zero mean Gaussian distribution with probability density function (PDF) $f_{ij} : \mathbb{R}^n \to \mathbb{R}^+$:

$$f_{ij}(\boldsymbol{y}_{ij}) = \frac{1}{(2\pi)^{n/2}\ \det(\boldsymbol{\Sigma}_{ij})^{1/2}} \exp(-\frac{1}{2}(\boldsymbol{y}_{ij}^\top \boldsymbol{\Sigma}_{ij}^{-1} \boldsymbol{y}_{ij})), \tag{2}$$

where $\boldsymbol{\Sigma}_{ij} = \delta_{ij}^2 \boldsymbol{I}_{n\times n},\ \delta_{ij}^2$ means the isotropic variance value.

For the edge in the rotation graph $(i, j) \in \mathcal{F}$, we have the noisy relative rotation measurement $\boldsymbol{H}_{ij} \in SO(n)$ between $\boldsymbol{R}_i$ and $\boldsymbol{R}_j$:

$$\boldsymbol{H}_{ij} = \boldsymbol{Z}_{ij}\boldsymbol{R}_j\boldsymbol{R}_i^\top, \tag{3}$$

where $\boldsymbol{Z}_{ij}$ is a random rotation of which distributed function $\widehat{f_{ij}} : SO(n) \to \mathbb{R}^+$ means an isotropic Langevin distribution with mean $\boldsymbol{I}_{n\times n}$ and concentration $\kappa_{ij} \geq 0$ [12]:

$$\begin{aligned} \widehat{f_{ij}}(\boldsymbol{Z}_{ij}) =& \frac{1}{c_n(\kappa_{ij})} \exp\left(\kappa_{ij}\ \text{trace}(\boldsymbol{Z}_{ij})\right), \\ c_2(\kappa_{ij}) =& I_0(2\kappa_{ij}), \\ c_3(\kappa_{ij}) =& \exp(\kappa_{ij})\left(I_0(2\kappa_{ij}) - I_1(2\kappa_{ij})\right), \\ I_v(2\kappa_{ij}) =& \frac{1}{2\pi}\int_{-\pi}^{\pi} \exp\left(2\kappa_{ij}\cos(\theta)\right)\cos(v\theta)d\theta, \end{aligned} \tag{4}$$

where $c_n(\kappa_{ij}),\ n = 2, 3$ is a normalization constant such that $\widehat{f_{ij}}$ has unit mass. $I_v(2\kappa_{ij}),\ v = \{0, 1, 2, \cdots\} \in \mathbb{Z}$ means the modified Bessel functions [35]. We write $\boldsymbol{Z}_{ij} \sim Lang(\boldsymbol{I}_{n\times n}, \kappa_{ij})$ to mean that $\boldsymbol{Z}_{ij}$ is a random rotation matrix with PDF (4). This PDF satisfies the assumptions shown in [12]: 1. smoothness and support; 2. independence; 3. bi-invariance.

Under the independence assumption of the measurements, the log-likelihood function of an estimand (parameters to be estimated) $\boldsymbol{\theta} = \boldsymbol{x} \times \boldsymbol{R} = (\boldsymbol{x}_0, \cdots, \boldsymbol{x}_{n_p}, \boldsymbol{R}_0, \cdots, \boldsymbol{R}_{n_p}) \in \mathcal{P}$, given the measurements $\boldsymbol{y} = \{\boldsymbol{p}_{ij},\ \boldsymbol{H}_{ij}, (i, j) \in \mathcal{E}\}$[1], is given by:

$$\begin{aligned} L(\boldsymbol{y}; \boldsymbol{\theta}) =& \sum_{(i,j)\in\mathcal{E}} \log f_{ij}(\boldsymbol{p}_{ij} - \boldsymbol{R}_i^\top(\boldsymbol{x}_j - \boldsymbol{x}_i)) \\ &+ \frac{1}{2}\sum_{(i,j)\in\mathcal{F}} \log \widehat{f_{ij}}(\boldsymbol{H}_{ij}\boldsymbol{R}_i\boldsymbol{R}_j^\top). \end{aligned} \tag{5}$$

[1]If an edge $(i, j) \in \mathcal{E}$, then there exists a corresponding edge $(i, j) \in \mathcal{F}$ for the rotation graph.

The coefficient $\frac{1}{2}$ is used to balance the information in the un-directed rotation graph $\mathcal{G}_1$ and the directed pose-graph $\mathcal{G}$, satisfying $(i, j) \in \mathcal{F} \Leftrightarrow j \in V_i$, and $\sum_{(i,j)\in\mathcal{F}} \log \widehat{f_{ij}}(\boldsymbol{H}_{ij}\boldsymbol{R}_i\boldsymbol{R}_j^\top) = \sum_i \sum_{j\in V_i} \log \widehat{f_{ij}}(\boldsymbol{H}_{ij}\boldsymbol{R}_i\boldsymbol{R}_j^\top) = 2\sum_{(i,j)\in\mathcal{E}} \log \widehat{f_{ij}}(\boldsymbol{H}_{ij}\boldsymbol{R}_i\boldsymbol{R}_j^\top)$.

By introducing the PDF functions (2), (4), finding the maximum of the log-likelihood function (5) is equivalent to:

$$\begin{aligned} \max_{\boldsymbol{\theta}\in\mathcal{P}} & \sum_{(i,j)\in\mathcal{E}} \kappa_{ij}\text{trace}(\boldsymbol{H}_{ij}\boldsymbol{R}_i\boldsymbol{R}_j^\top) \\ - & \sum_{(i,j)\in\mathcal{E}} \frac{\delta_{ij}^{-2}}{2}\|\boldsymbol{p}_{ij} - \boldsymbol{R}_i^\top(\boldsymbol{x}_j - \boldsymbol{x}_i)\|_2^2. \end{aligned} \tag{6}$$

C. Geometry of the parameter spaces

The FIM is a classical tool for estimation problems on Euclidean spaces. In order to define the FIM on a manifold $\mathbb{R}^n \times SO(n),\ n = 2, 3$, we need to define some notions and tools to describe the parameter spaces for the synchronization.

1) Tangent space on $SO(n)$ [36]: As a Lie group, the dimension of its minimal representation is $d = d(n) = \frac{n(n-1)}{2}$ ($d = 1$ and 3, for 2D and 3D case). We can admit a tangent space $\mathcal{T}_{\boldsymbol{Q}}SO(n),\ n = 2, 3$ for each rotation:

$$\mathcal{T}_{\boldsymbol{Q}}SO(n) = \boldsymbol{Q}so(n) \triangleq \{\boldsymbol{Q}\boldsymbol{\Omega} : \boldsymbol{\Omega} \in \mathbb{R}^{n\times n}, \boldsymbol{\Omega}^\top + \boldsymbol{\Omega} = 0\}, \tag{7}$$

where $\boldsymbol{Q} \in SO(n)$, $so(n)$ is the Lie algebra corresponding to $SO(n)$.

2) Inner product on $\mathbb{R}^n$ and $SO(n)$ [12]: Based on the Riemannian metric of the manifold $\mathbb{R}^n \times SO(n)$, we define the inner products on the tangent spaces of $\mathbb{R}^n$ and $SO(n)$ respectively:

$$\begin{cases} \langle\boldsymbol{\rho}_1, \boldsymbol{\rho}_2\rangle_{\boldsymbol{X}} = \boldsymbol{\rho}_1^\top\boldsymbol{\rho}_2 & \boldsymbol{\rho}_1, \boldsymbol{\rho}_2 \in \mathbb{R}^n \\ \langle\boldsymbol{\Omega}_1, \boldsymbol{\Omega}_2\rangle_{\boldsymbol{R}} = \text{trace}(\boldsymbol{\Omega}_1^\top\boldsymbol{\Omega}_2) & \boldsymbol{\Omega}_1, \boldsymbol{\Omega}_2 \in \mathcal{T}_{\boldsymbol{Q}}SO(n). \end{cases} \tag{8}$$

Because $(\boldsymbol{Q}\boldsymbol{\Omega}_1)^\top\boldsymbol{Q}\boldsymbol{\Omega}_2 = \boldsymbol{\Omega}_1^\top\boldsymbol{\Omega}_2$, we omit the tangent subscripts $\boldsymbol{Q}$ in above equation and all related inner product equations of this paper, for better readability. The Riemannian metric of $\mathbb{R}^n \times SO(n)$ is the sum of the Riemannian metrics of $\mathbb{R}^n$ and $SO(n)$, which helps to maintain the bi-invariance property. $\forall(\boldsymbol{\rho}, \boldsymbol{Q}) \in \mathbb{R}^n \times SO(n),\ \forall(\boldsymbol{\rho}_i, \boldsymbol{\Omega}_i) \in \mathcal{T}_{(\boldsymbol{\rho},\boldsymbol{Q})}(\mathbb{R}^n \times SO(n)),\ i = 1, 2$, the specific expression of the Riemannian metric of $\mathbb{R}^n \times SO(n)$ is defined as:

$$\langle(\boldsymbol{\rho}_1, \boldsymbol{\Omega}_1), (\boldsymbol{\rho}_2, \boldsymbol{\Omega}_2)\rangle := \langle\boldsymbol{\rho}_1, \boldsymbol{\rho}_2\rangle_{\boldsymbol{X}} + \langle\boldsymbol{\Omega}_1, \boldsymbol{\Omega}_2\rangle_{\boldsymbol{R}}. \tag{9}$$

3) Gradient on $SO(n)$ [37]: Let $h : SO(n) \to \mathbb{R}$ be a differentiable function, we can define the gradient of h by:

$$\begin{aligned} \text{grad } h(\boldsymbol{Q}) &= \boldsymbol{Q}\text{skew}(\boldsymbol{Q}^\top\nabla h(\boldsymbol{Q})), \\ \text{skew}(\star) &\triangleq (\star - \star^\top)/2, \end{aligned} \tag{10}$$

where $\nabla h(\boldsymbol{Q})$ means the gradient of h seen as a Euclidean function in $\mathbb{R}^{n\times n}$.

The directional derivative of h at $\boldsymbol{Q}$ along $\boldsymbol{Q}\boldsymbol{\Omega}$ can be written as:

$$\langle\text{grad } h(\boldsymbol{Q}), \boldsymbol{Q}\boldsymbol{\Omega}\rangle_{\boldsymbol{R}}, \tag{11}$$

where $\boldsymbol{Q}\boldsymbol{\Omega}$ is a tangent vector in the tangent space.

D. Definition of FIM

Definition [12]: Let $\boldsymbol{\theta} \in \mathcal{P}$ be unknown parameter and $f(\boldsymbol{y};\boldsymbol{\theta})$ be the PDF of the measurement $\boldsymbol{y}$ conditioned by $\boldsymbol{\theta}$ (in this paper, the measurement noises are shown in the PDFs (2) and (4)). Based on the log-likelihood function $L(\boldsymbol{y};\boldsymbol{\theta}) = \log f(\boldsymbol{y};\boldsymbol{\theta})$ shown in (5) and the orthonormal basis, the (i,j)-th element of the FIM is defined as:

$$\boldsymbol{F}_{(i,j)} = \mathbb{E}\left\{\langle \text{grad}L(\boldsymbol{y};\boldsymbol{\theta}), e_i\rangle \cdot \langle \text{grad}L(\boldsymbol{y};\boldsymbol{\theta}), e_j\rangle\right\}, \quad (12)$$

where e_i and e_j are the i-th and j-th bases of the tangent space of the parameters. Expectations are taken w.r.t. the measurement $\boldsymbol{y}$. They will be defined based on the parameter space [1]. It is noted that the FIM is directly decided by the bases. For a parameter space, there may exist different bases.

IV. FIM FOR 2D POSE-GRAPH SLAM

In this section, focused on 2D pose-graph SLAM, we will show its basis and FIM. Some further discussions are also presented to compare with some previous work.

A. Geometry of the parameter spaces for $\mathbb{R}^2 \times SO(2)$

As shown in Section III-C, the tools, including the tangent space, the inner product, and the gradient, are defined for both the 2D ($\mathbb{R}^2 \times SO(2)$) and 3D ($\mathbb{R}^3 \times SO(3)$) parameter space. In this part, we will show the basis for the group $\mathbb{R}^2 \times SO(2)$, which is needed for the derivation of the FIM.

In 2D case, define[2]:

$$\boldsymbol{E} = \begin{bmatrix} 0 & -1 \\ 1 & 0 \end{bmatrix}, \quad (13)$$

the orthogonal basis $\boldsymbol{E}^{\boldsymbol{x},\boldsymbol{R}} = (\boldsymbol{E}^{\boldsymbol{x}}_{0,1}, \boldsymbol{E}^{\boldsymbol{x}}_{0,2} \cdots, \boldsymbol{E}^{\boldsymbol{x}}_{n_p,1}, \boldsymbol{E}^{\boldsymbol{x}}_{n_p,2}, \boldsymbol{E}^{\boldsymbol{R}}_{0}, \cdots, \boldsymbol{E}^{\boldsymbol{R}}_{n_p})$ of the tangent space $\mathcal{T}_{(\boldsymbol{x},\boldsymbol{R})}\mathcal{P}$ can be fixed as:

$$\begin{aligned}
\boldsymbol{E}^{\boldsymbol{x}}_{i,k} &= ({\boldsymbol{E}^{X}_{i,k}}^{\top}; \boldsymbol{0}_{2(n_p+1)\times 2}),\ i \in \{0,\ 1, \cdots,\ n_p\},\ k = 1,2 \\
\boldsymbol{E}^{\boldsymbol{R}}_{j} &= (\boldsymbol{0}_{2(n_p+1)\times 1}; {\boldsymbol{E}^{R}_{j}}^{\top}),\ j \in \{0,\ 1, \cdots,\ n_p\}, \\
\boldsymbol{E}^{X}_{i,k} &= (\boldsymbol{0}_{1\times 2}, \cdots, \boldsymbol{0}_{1\times 2}, \underbrace{1}_{k-\text{th}}, 0, \boldsymbol{0}_{1\times 2}, \cdots, \boldsymbol{0}_{1\times 2})_{1\times 2(n_p+1)}, \\
&\qquad\qquad\qquad\qquad\qquad\qquad\qquad\qquad\quad \underbrace{\qquad}_{i-\text{th}} \\
\boldsymbol{E}^{R}_{j} &= (\boldsymbol{0}_{2\times 2}, \cdots, \boldsymbol{0}_{2\times 2}, \underbrace{\boldsymbol{R}_j\boldsymbol{E}}_{j-\text{th}}, \boldsymbol{0}_{2\times 2}, \cdots, \boldsymbol{0}_{2\times 2})_{2\times 2(n_p+1)},
\end{aligned} \quad (14)$$

where $\boldsymbol{E}^{\boldsymbol{x}}_{i,k}$ and $\boldsymbol{E}^{\boldsymbol{R}}_{j}$ are corresponding to the k-axis coordinate of the i-th pose $(\boldsymbol{x}_i, \boldsymbol{R}_i)$ and the rotation parameter of the j-th pose $(\boldsymbol{x}_j, \boldsymbol{R}_j)$.

[2]It is noted that, for 2D case, we present the FIM using the orthogonal basis but not the orthonormal basis (orthonormal is a subset of orthogonal). Commonly, in the FIM definition (12), the basis used is the orthonormal basis. However, in most SLAM methods [38], [39], the rotation matrix is represented by the minimal representation vectors $\boldsymbol{\phi}$ ($\exp(\boldsymbol{\phi}^{\wedge})$ is the corresponding rotation matrix, where $\star^{\wedge}$ means the skew-symmetric matrix of $\star$), which means that, for simplicity, the orthogonal basis (13) (14) is used in the 2D case. Moreover, for the 2D rotation matrix, its corresponding Euler angle value is approximately equal to the minimal Lie group representation using the basis (13) (14). Thus for the 2D case in this paper, we present the results using this orthogonal basis (13) (14) corresponding to the Euler angle. If using the orthonormal basis $\boldsymbol{E}/\sqrt{2}$, the derivation process is similar and the weight values $w^{SO(2)}_{ij}$ and ψ_i for rotation group part in the FIM (15) will be $w^{SO(2)}_{ij}/2$ and $\psi_i/2$.

B. FIM

Because of the group $\mathbb{R}^2 \times SO(2)$, there are four different parts in the FIM: One sub-matrix corresponding to the Euclidean space $\mathbb{R}^2$. One sub-matrix corresponding to $SO(2)$ Lie group, and other two sub-matrices related to the coupling part of $\mathbb{R}^2$ Euclidean space and $SO(2)$ Lie group. Based on the definition (12), we can prove the following theorem:

Theorem 1. *For the 2D case of the pose graph problem* (6)*, given the basis* (14)*, the FIM is:*

$$\boldsymbol{\mathcal{I}}_{2D} = \left[\begin{array}{c|c} \boldsymbol{L}^{\mathbb{R}^2}_{w} & \triangle^{\top}_{w} \\ \hline \triangle_{w} & \boldsymbol{L}^{SO(2)}_{w} + diag\{\psi_1, \cdots, \psi_{n_p}\} \end{array}\right], \quad (15)$$

where $\boldsymbol{L}^{\mathbb{R}^2}_{w}$ is the sub-FIM corresponding to the Euclidean space $\mathbb{R}^2$, satisfying $\boldsymbol{L}^{\mathbb{R}^2}_{w} = \boldsymbol{L}_{w_{\mathbb{R}}} \otimes \boldsymbol{I}_{2\times 2}$. $\boldsymbol{L}_{w_{\mathbb{R}}}$ is the weighted Laplacian matrix, of which weight value $w^{\mathbb{R}}_{ij}$ for (i,j)-th edge is δ^{-2}_{ij}; $\boldsymbol{L}^{SO(2)}_{w} + diag\{\psi_1, \cdots, \psi_{n_p}\}$ is the sub-FIM corresponding to the $SO(2)$ Lie group, satisfying $\boldsymbol{L}^{SO(2)}_{w} = \boldsymbol{L}_{w_{SO(2)}} \otimes \boldsymbol{I}_{d\times d}$, where d is given in Section III-C1. $\boldsymbol{L}_{w_{SO(2)}}$ is the weighted Laplacian matrix, of which weight value $w^{SO(2)}_{ij}$ for (i,j)-th edge is $2\kappa_{ij}\frac{I_1(2\kappa_{ij})}{I_0(2\kappa_{ij})}$. $\psi_i = \sum_{j\in V^+_i} \delta^{-2}_{ij}\|\boldsymbol{x}_i - \boldsymbol{x}_j\|^2_2,\ i = 1,2,\cdots,n_p$; The (i,i_1)-th block of the $SO(2)$ by $\mathbb{R}^2$ coupling sub-matrix $\triangle_w$ corresponding to the $(n_p + 1 + i, i_1)$-th block of the FIM is:

$$(\triangle_w)_{i,i_1} = \begin{cases} \sum_{j\in V^+_i} \delta^{-2}_{ij}(\boldsymbol{x}_i - \boldsymbol{x}_j)^{\top}\boldsymbol{E} & i = i_1 \\ \delta^{-2}_{ii_1}(\boldsymbol{x}_{i_1} - \boldsymbol{x}_i)^{\top}\boldsymbol{E} & (i,i_1) \in \mathcal{E} \\ \boldsymbol{0}_{1\times 2} & else. \end{cases} \quad (16)$$

Proof: See Appendix A in supplementary material [40]. ■

Remark 1. *It is noted that, for 2D pose-graph SLAM, if the first node $(\boldsymbol{x}_0,\ \boldsymbol{R}_0)$ is anchored, the rows and columns corresponding to node $(\boldsymbol{x}_0,\ \boldsymbol{R}_0)$ of the FIM need to be deleted. So the FIM of the SLAM problem is related to the weighted reduced Laplacian matrix.*

C. Discussion on the FIM for 2D pose-graph SLAM

In the previous 2D work [5], [6] and [34], based on the block-isotropic Gaussian noise and the Euler angle, we get a similar formulation of the FIM by: $\boldsymbol{\mathcal{I}}_{2D} = \boldsymbol{J}^{\top}\boldsymbol{\Sigma}^{-1}_{2D}\boldsymbol{J}$, where $\boldsymbol{J}$ is the Jacobian matrix of the factors of the pose-graph SLAM, $\boldsymbol{\Sigma}_{2D}$ is the block-diagonal matrix whose non-zero blocks are the covariances of the factors of the 2D pose-graph SLAM. In fact, there are three important differences between this work with the previous work [5], [6], [34]:

a) Different noise assumptions: The noise for the rotation part used in this work is different from the Gaussian noise. For the Gaussian noise, we have following result: If $\boldsymbol{x} \sim \mathcal{N}(\boldsymbol{\mu}, \boldsymbol{P})$, we can get $\boldsymbol{G}\boldsymbol{x} \sim \mathcal{N}(\boldsymbol{G}\boldsymbol{\mu}, \boldsymbol{G}\boldsymbol{P}\boldsymbol{G}^{\top})$. So the FIM can be computed by $\boldsymbol{J}^{\top}\boldsymbol{\Sigma}^{-1}_{2D}\boldsymbol{J}$. This equation may not be suitable for other kinds of noises, so we need to compute the FIM based on its general definition shown in (12).

b) Lie group representation instead of Euler angle: The previous work [5], [6], [34] is built based on the Euler angle representation for the orientation of the poses. The measurement of the rotation part is simply written as the subtraction of the orientation. Because of the non-uniqueness of the Euler angle and the periodicity of the trigonometric functions, the wraparound problem will lead the measurement function to be complex instead of a simple subtraction. In this work, the formulation is built based on the rotation group, so there is no wraparound issue.

c) Expandability of results from 2D to 3D: Based on the Gaussian noise on the Euler angle, for the 3D case, the relative pose measurement can not be written as a simple subtraction formulation, which is greatly different from the 2D case, so the expandability of the original method is limited in 2D case. Based on the rigorous treatment of uncertainty on $\mathbb{R}^n \times SO(n)$ (isotropic Langevin noise for rotation and block-isotropic Gaussian noise for translation), the similar but more complex results are obtained rigorously in the 2D case and further extended into the 3D case in the following section.

V. FIM FOR 3D POSE-GRAPH SLAM

In this section, we will present the orthonormal basis and the FIM for 3D pose-graph SLAM.

A. Geometry of the parameter spaces for $\mathbb{R}^3 \times SO(3)$

In 3D case, define[3]:

$$\boldsymbol{E}_1 = \frac{1}{\sqrt{2}}\begin{bmatrix} 0 & 0 & 0 \\ 0 & 0 & 1 \\ 0 & -1 & 0 \end{bmatrix}, \boldsymbol{E}_2 = \frac{1}{\sqrt{2}}\begin{bmatrix} 0 & 0 & -1 \\ 0 & 0 & 0 \\ 1 & 0 & 0 \end{bmatrix}, \boldsymbol{E}_3 = \frac{1}{\sqrt{2}}\begin{bmatrix} 0 & 1 & 0 \\ -1 & 0 & 0 \\ 0 & 0 & 0 \end{bmatrix}, \tag{17}$$

the orthonormal basis $\boldsymbol{E}^{\boldsymbol{x},\boldsymbol{R}} = (\boldsymbol{E}^{\boldsymbol{x}}_{0,1}, \boldsymbol{E}^{\boldsymbol{x}}_{0,2}, \boldsymbol{E}^{\boldsymbol{x}}_{0,3}, \cdots, \boldsymbol{E}^{\boldsymbol{x}}_{n_p,1}, \boldsymbol{E}^{\boldsymbol{x}}_{n_p,2}, \boldsymbol{E}^{\boldsymbol{x}}_{n_p,3}, \boldsymbol{E}^{\boldsymbol{R}}_{0,1}, \boldsymbol{E}^{\boldsymbol{R}}_{0,2}, \boldsymbol{E}^{\boldsymbol{R}}_{0,3}, \cdots, \boldsymbol{E}^{\boldsymbol{R}}_{n_p,1}, \boldsymbol{E}^{\boldsymbol{R}}_{n_p,2}, \boldsymbol{E}^{\boldsymbol{R}}_{n_p,3})$ of the tangent space $\mathcal{T}_{(\boldsymbol{x},\boldsymbol{R})}\mathcal{P}$ can be fixed as:

$$\begin{aligned}
&\boldsymbol{E}^{\boldsymbol{x}}_{i,k} = (\boldsymbol{E}^{X}_{i,k}{}^{\top}; \boldsymbol{0}_{9(n_p+1)\times 3}),\ i \in \{0, \cdots,\ n_p\},\ k = 1,2,3,\\
&\boldsymbol{E}^{\boldsymbol{R}}_{j,k} = (\boldsymbol{0}_{3(n_p+1)\times 1}; \boldsymbol{E}^{R}_{j,k}{}^{\top}),\ j \in \{0, \cdots,\ n_p\},\\
&\boldsymbol{E}^{X}_{i,k} = (\boldsymbol{0}_{1\times 3}, \cdots, \boldsymbol{0}_{1\times 3}, \underbrace{\underbrace{1}_{k-\text{th}}}_{i-\text{th}}, 0, 0, \boldsymbol{0}_{1\times 3}, \cdots, \boldsymbol{0}_{1\times 3})_{1\times 3(n_p+1)},\\
&\boldsymbol{E}^{R}_{j,k} = (\boldsymbol{0}_{3\times 3}, \cdots, \boldsymbol{0}_{3\times 3}, \underbrace{\boldsymbol{R}_j\boldsymbol{E}_k}_{3j+k-\text{th}}, \boldsymbol{0}_{3\times 3}, \cdots, \boldsymbol{0}_{3\times 3})_{3\times 9(n_p+1)}.
\end{aligned} \tag{18}$$

B. FIM

Similar to the FIM in Section IV-B, there are four parts in the FIM for the group $\mathbb{R}^3 \times SO(3)$ of the rigid body motions in 3D space. Based on the definition (12), we can prove the following theorem:

Theorem 2. *For the 3D case of the pose graph problem* (6)*, given the orthonormal basis* (18)*, the FIM is:*

$$\boldsymbol{\mathcal{I}}_{3D} = \left[\begin{array}{c|c} \boldsymbol{L}^{\mathbb{R}^3}_w & \triangle^{3D\top}_w \\ \hline \triangle^{3D}_w & \boldsymbol{L}^{SO(3)}_w + diag\{\boldsymbol{\Psi}_1, \cdots, \boldsymbol{\Psi}_{n_p}\} \end{array}\right], \tag{19}$$

where $\boldsymbol{L}^{\mathbb{R}^3}_w$ is the sub-FIM corresponding to the Euclidean space $\mathbb{R}^3$, satisfying $\boldsymbol{L}^{\mathbb{R}^3}_w = \boldsymbol{L}_{w_{\mathbb{R}}} \otimes \boldsymbol{I}_{3\times 3}$. $\boldsymbol{L}_{w_{\mathbb{R}}}$ is the same as that in Theorem 1; $\boldsymbol{L}^{SO(3)}_w + diag\{\boldsymbol{\Psi}_1, \cdots, \boldsymbol{\Psi}_{n_p}\}$ is the sub-FIM corresponding to the $SO(3)$ Lie group, satisfying $\boldsymbol{L}^{SO(3)}_w = \boldsymbol{L}_{w_{SO(3)}} \otimes \boldsymbol{I}_{d\times d}$, where d is given in Section III-C1. $\boldsymbol{L}_{w_{SO(3)}}$ is the weighted Laplacian matrix, of which weight value $w^{SO(3)}_{ij}$ for (i,j)-th edge is $\frac{1}{3}\frac{\kappa^2_{ij}(2I_0(2\kappa_{ij}) - I_1(2\kappa_{ij}) - 2I_2(2\kappa_{ij}) + I_3(2\kappa_{ij}))}{2I_0(2\kappa_{ij}) - 2I_1(2\kappa_{ij})}$. $\boldsymbol{\Psi}_i$ satisfies:

$$\begin{aligned}
&\boldsymbol{\Psi}_i = \begin{bmatrix} \psi^{11}_i & \psi^{12}_i & \psi^{13}_i \\ \psi^{12}_i & \psi^{22}_i & \psi^{21}_i \\ \psi^{13}_i & \psi^{21}_i & \psi^{33}_i \end{bmatrix},\ i = 1,2,\cdots,n_p\\
&\psi^{kl}_i = \sum_{j\in V^+_i} \delta^{-2}_{ij}(\boldsymbol{x}_i - \boldsymbol{x}_j)^\top \boldsymbol{R}_i \boldsymbol{I}^{k,l}_{3\times 3} \boldsymbol{R}^\top_i (\boldsymbol{x}_i - \boldsymbol{x}_j);
\end{aligned} \tag{20}$$

Let $\boldsymbol{\varsigma}^k_{ij} = (\delta^{-2}_{ij}(\boldsymbol{x}_i - \boldsymbol{x}_j)^\top \boldsymbol{R}_i \boldsymbol{E}_k \boldsymbol{R}^\top_i)^\top$, $k = 1,2,3$, we have the (i,i_1)-th block of the $SO(3)$ by $\mathbb{R}^3$ coupling sub-matrix $\triangle^{3D}_w$ corresponding to the (n_p+1+i,i_1)-th block of the FIM:

$$(\triangle^{3D}_w)_{i,i_1} = \begin{cases} \begin{bmatrix} \sum_{j\in V^+_i}\boldsymbol{\varsigma}^1_{ij} & \sum_{j\in V^+_i}\boldsymbol{\varsigma}^2_{ij} & \sum_{j\in V^+_i}\boldsymbol{\varsigma}^3_{ij} \end{bmatrix}^\top & i = i_1 \\ \begin{bmatrix} -\boldsymbol{\varsigma}^1_{ii_1} & -\boldsymbol{\varsigma}^2_{ii_1} & -\boldsymbol{\varsigma}^3_{ii_1} \end{bmatrix}^\top & (i,i_1) \in \mathcal{E} \\ \boldsymbol{0}_{3\times 3} & \textit{else}. \end{cases} \tag{21}$$

Proof: See Appendix B in supplementary material [40]. ■

Similarly, for the 3D case, if the first node is anchored, the corresponding rows and columns of the FIM need to be deleted. So the anchored FIM is related to the weighted reduced Laplacian matrix. The following CRLB and discussions on optimality metrics are focused on the pose-graph SLAM, so the FIM is defined based on the anchored situation.

VI. CRLB FOR POSE-GRAPH SLAM

Classical CRLB gives a lower bound on the covariance matrix $\boldsymbol{C}$ of any unbiased estimator for an estimation problem in $\mathbb{R}^n$. In terms of the FIM $\boldsymbol{F} = \boldsymbol{\mathcal{I}}_{nD},\ n = 2,3$ of that problem, the classical result reads $\boldsymbol{C} \succeq \boldsymbol{F}^{-1}$. However, because our parameter space $\mathcal{P}$ is a manifold instead of a flat Euclidean space, the CRLB takes up the more general form $\boldsymbol{C} \succeq \boldsymbol{F}^{-1} +$ curvature terms [23].

Inspired by [12], we also show that when the signal-to-noise ratio (SNR) is large enough, the curvature terms will become negligible. The CRLB is the asymptotic bound, which means only the leading-order curvature term has been computed. For SLAM, the non-flat property of the parameter space comes

[3]Similar to the 2D case, in many applications, $\sqrt{2}\boldsymbol{E}_1$, $\sqrt{2}\boldsymbol{E}_2$, $\sqrt{2}\boldsymbol{E}_3$ are used in the bases of the manifold SO(3). In that case, the weight for rotation group part in the final FIM will be $2w^{SO(3)}_{ij}$.

from the rotation group, so, in order to limit the Taylor truncation error, the SNR snr is heuristicly defined as[4]:

$$snr = \frac{(n_p + 1 - |\mathcal{A}|)\mathbb{E}\{\text{dist}^2(\boldsymbol{Z}_{uni}^{\boldsymbol{R}}, \boldsymbol{I}_{3\times 3})\}}{9\text{trace}(\boldsymbol{I}^{SO(3)^{-1}})}, \tag{22}$$

where $\boldsymbol{I}^{SO(3)^{-1}}$ is the sub-matrix of the inverse function of the FIM $\boldsymbol{\mathcal{I}}_{3D}{}^{-1}$ corresponding to the $SO(3)$ Lie group, $|\mathcal{A}|$ means the number of anchored nodes (in general $|\mathcal{A}| = 1$ for SLAM), the expectation is taken w.r.t. $\boldsymbol{Z}_{uni}^{\boldsymbol{R}}$, uniformly distributed over $SO(3)$. For the numerator, $n_p+1-|\mathcal{A}|$ means the number of the estimated poses and $\mathbb{E}\{\text{dist}^2(\boldsymbol{Z}_{uni}^{\boldsymbol{R}}, \boldsymbol{I}_{3\times 3})\}$ shows a suitable constant, which means the expected squared-error for a bad rotational estimator based on some uniformly random measurements (no information is available in the random estimator). The denominator is defined because the SNR is inversely proportional to the trace of the the rotational block of the inverse matrix of the FIM. When the quantity of the rotational measurements increases (large-scale $\boldsymbol{I}^{SO(3)}$), the SNR snr will be large. It is well-known that it's the rotational part specifically that makes the SLAM problem nontrivial. When the robot orientation is assumed to be known, the SLAM problem can be simplified as a linear-Gaussian estimation problem, called Compass-SLAM problem [6], whose globally-optimal solution can be computed easily by solving a linear least squares problem and the curvature terms will be zero. Hence, we do not consider anything about the performance of the position estimates in the defined SNR (22) since the position estimate has no effect on the curvature term.

A. CRLB for 2D pose-graph SLAM

Before the discussion about the CRLB of the synchronization of the manifolds $\mathbb{R}^2 \times SO(2)$, we introduce a lemma [41]:

Lemma 1. *Let $\mathcal{M} = \mathcal{M}_1 \times \mathcal{M}_2$ be the product of two Riemannian manifolds, R be its curvature tensor, and R_1, R_2 be curvature tensors for $\mathcal{M}_1$ and $\mathcal{M}_2$ respectively, then one can relate R, R_1 and R_2 by:*

$$R(X, Y) = R_1(X_1, Y_1) + R_2(X_2, Y_2), \tag{23}$$

where $X_i, Y_i \in \mathcal{T}(\mathcal{M}_i), i = 1, 2$ and $X = X_1 + X_2, Y = Y_1 + Y_2 \in \mathcal{T}(\mathcal{M})$, $\mathcal{T}(\star)$ means the tangent space of $\star$.

Based on Lemma 1, we can prove that the curvature tensor of the parameter space $\mathcal{P}_1 = \{\mathbb{R}^2 \times \cdots \times \mathbb{R}^2\}_{n_p} \times \{SO(2) \times \cdots \times SO(2)\}_{n_p}$ is equal to the sum of the multiple curvature tensors of the group $\{\mathbb{R}^2 \times \cdots \times \mathbb{R}^2\}_{n_p}$ and the group $\{SO(2) \times \cdots \times SO(2)\}_{n_p}$. As the (product) Lie group, the curvature tensors of the parameter space $\mathcal{P}_1$ on the tangent space $\mathcal{T}_{(\boldsymbol{x},\boldsymbol{R})}\mathcal{P}_1$ is given by a simple formula [12]:

$$\langle R(\bar{\boldsymbol{X}}, \bar{\boldsymbol{\Omega}})\bar{\boldsymbol{\Omega}},\ \bar{\boldsymbol{X}}\rangle = \frac{1}{4}\|[\bar{\boldsymbol{X}}, \bar{\boldsymbol{\Omega}}]\|_F^2, \tag{24}$$

where $[\bar{\boldsymbol{X}}, \bar{\boldsymbol{\Omega}}]$ is the Lie bracket of $\bar{\boldsymbol{X}}$ and $\bar{\boldsymbol{\Omega}}$, two vectors (not necessarily orthonormal) in the tangent space $\mathcal{T}_{(\boldsymbol{x},\boldsymbol{R})}\mathcal{P}_1$. Because of the Lie brackets and the bases (14), it is easy to find that these two groups are both flat and their curvature tensors are $\mathbf{0}$. So the curvature tensor of the space $\mathcal{P}_1$ is $\mathbf{0}$.

The CRLB for 2D pose-graph SLAM on $\mathbb{R}^2 \times SO(2)$ is:

$$\boldsymbol{C} \succeq \boldsymbol{F}^{-1} + \text{curvature terms} = \boldsymbol{F}^{-1} + \mathbf{0} = \boldsymbol{F}^{-1}. \tag{25}$$

So we can see that, for the parameter space $\mathcal{P}_1$, its CRLB formula is the same as the classical CRLB result for the flat Euclidean space shown as $\boldsymbol{C} \succeq \boldsymbol{F}^{-1}$.

B. CRLB for 3D pose-graph SLAM

Different from the $\mathbb{R}^2 \times SO(2)$ group, the manifold $\mathbb{R}^3 \times SO(3)$ is not a flat space. So we need to compute the curvature terms. Based on Lemma 1, we known that the curvature tensor of the parameter space $\mathcal{P}_3 = \{\mathbb{R}^3 \times \cdots \times \mathbb{R}^3\}_{n_p} \times \{SO(3) \times \cdots \times SO(3)\}_{n_p}$ is equal to the sum of the curvature tensor of the manifold $\{\mathbb{R}^3 \times \cdots \times \mathbb{R}^3\}_{n_p}$ and the manifold $\mathcal{P}_2 = \{SO(3) \times \cdots \times SO(3)\}_{n_p}$. The Euclidean space $\mathbb{R}^3$ is flat with a $\mathbf{0}$ curvature tensor, so the curvature tensor of the space $\mathcal{P}_3$ is determined by the curvature tensor of the manifold $\mathcal{P}_2$.

Based on Theorem 4 in [23], CRLB follows: $\boldsymbol{C} \geq \boldsymbol{F}^{-1} - \frac{1}{3}(R_m(\boldsymbol{F}^{-1})\boldsymbol{F}^{-1} + \boldsymbol{F}^{-1}R_m(\boldsymbol{F}^{-1}))$, where the operator R_m: $\mathbb{R}_{6n_p\times 6n_p} \rightarrow \mathbb{R}_{6n_p\times 6n_p}$ involves the Riemannian curvature tensor of the parameter space. The operator $R_m(\boldsymbol{F}^{-1}) = \frac{1}{4}\text{diag}\{\mathbf{0}, \text{ddiag}(\boldsymbol{I}^{SO(3)^{-1}})\}$ of the parameter space $\mathcal{P}_2$ for the anchored rotation synchronization has been shown by [12].

Following the same formulation as in [12], we can get the curvature tensor of 3D pose-graph SLAM:

$$\begin{aligned} \boldsymbol{C} &\succeq \boldsymbol{F}^{-1} - \frac{1}{12}(\text{ddiag}(\widetilde{\boldsymbol{L}})\boldsymbol{F}^{-1} + \boldsymbol{F}^{-1}\text{ddiag}(\widetilde{\boldsymbol{L}})), \\ \widetilde{\boldsymbol{L}} &= \begin{bmatrix} \mathbf{0} & \mathbf{0} \\ \mathbf{0} & \boldsymbol{I}^{SO(3)^{-1}} \end{bmatrix}_{6n_p\times 6n_p}. \end{aligned} \tag{26}$$

It is easy to find that when snr is large enough, compared with $\boldsymbol{F}^{-1}$, the function $\text{ddiag}(\widetilde{\boldsymbol{L}})\boldsymbol{F}^{-1} + \boldsymbol{F}^{-1}\text{ddiag}(\widetilde{\boldsymbol{L}})$ is much smaller. So it is negligible.

VII. Optimal experimental design metrics for pose-graph SLAM

In this section, we will discuss and compare the T-/D-optimal design metrics of 2D/3D pose-graph SLAM and show the tight bounds of these metrics.

A. T-optimality design metric

1) T-optimality design metric for the 2D case: T-optimality criterion maximizes the trace of the FIM. Based on the 2D FIM (15), we can get its T-optimality design metric:

$$\text{trace}(\boldsymbol{\mathcal{I}}_{2D}) = \text{trace}(\boldsymbol{L}_w^{\mathbb{R}^2}) + \text{trace}(\boldsymbol{L}_w^{SO(2)}) + \sum_{i=1}^{n_p}\psi_i. \tag{27}$$

[4]Because the SNR will be used in the 3D case only, we only show the formulation for 3D pose-graph.

2) T-optimality design metric for the 3D case: Based on the 3D FIM (19), the T-optimality design metric is:

$$\text{trace}(\boldsymbol{\mathcal{I}}_{3D}) = \text{trace}(\boldsymbol{L}_w^{\mathbb{R}^3}) + \text{trace}(\boldsymbol{L}_w^{SO(3)}) + \sum_{i=1}^{n_p} \text{trace}(\boldsymbol{\Psi}_i). \tag{28}$$

We can find that, in these three parts, only one part $\sum_{i=1}^{n_p} \text{trace}(\boldsymbol{\Psi}_i)$ includes the state vector $\boldsymbol{x}_i,\ \boldsymbol{x}_j,\ \boldsymbol{R}_i$. In fact, because of the special structure about $\boldsymbol{\Psi}_i$, we have: $\sum_{i=1}^{n_p} \text{trace}(\boldsymbol{\Psi}_i) = \sum_{i=1}^{n_p} \sum_{j\in V_i^+} \delta_{ij}^{-2} \|\boldsymbol{x}_j - \boldsymbol{x}_i\|_2^2$. The proof is shown in Appendix F of supplementary material [40].

3) Further analysis: We know that the measurement function is: $\boldsymbol{p}_{ij} = \boldsymbol{R}_i^\top (\boldsymbol{x}_j - \boldsymbol{x}_i) + \boldsymbol{y}_{ij}$. In general, we have:

$$\delta_{ij}^{-2} \|\boldsymbol{x}_j - \boldsymbol{x}_i\|_2^2 = \delta_{ij}^{-2} \|\boldsymbol{p}_{ij} - \boldsymbol{y}_{ij}\|_2^2 \approx \delta_{ij}^{-2} \|\boldsymbol{p}_{ij}\|_2^2. \tag{29}$$

Introduce (29) into the T-optimality metric (27) and (28), we have:

$$\begin{aligned} &\text{trace}(\boldsymbol{\mathcal{I}}_{nD}) \approx \text{trace}(\boldsymbol{L}_w^{\mathbb{R}^n}) + \text{trace}(\boldsymbol{L}_w^{SO(n)}) \\ &+ \sum_{i=1}^{n_p} \sum_{j\in V_i^+} \delta_{ij}^{-2} \|\boldsymbol{p}_{ij}\|_2^2,\ n = 2, 3. \end{aligned} \tag{30}$$

Based on this approximation (30), we can see that the trace of the FIM is weakly related to the state vector obtained by the estimated result. So, in general, the T-optimality metric can be easily computed using above equation without considering the SLAM result. For many real-word datasets, compared with the other parts, $\sum_{i=1}^{n_p} \sum_{j\in V_i^+} \delta_{ij}^{-2} \|\boldsymbol{p}_{ij}\|_2^2$ or $\sum_{i=1}^{n_p} \sum_{j\in V_i^+} \delta_{ij}^{-2} \|\boldsymbol{x}_j - \boldsymbol{x}_i\|_2^2$ is relatively small. So we have:

$$\begin{aligned} &\text{trace}(\boldsymbol{\mathcal{I}}_{nD}) \to \text{trace}(\boldsymbol{L}_w^{\mathbb{R}^n}) + \text{trace}(\boldsymbol{L}_w^{SO(n)}) \\ &= \sum_{i=1}^{n_p} \sum_{j\in V_i} \left(dw_{ij}^{SO(n)} + nw_{ij}^{\mathbb{R}} \right). \end{aligned} \tag{31}$$

B. D-optimality design metric

D-optimality design is to use the log-determinant of the covariance matrix as an objective function. However, the determinant of a high-dimensional dense matrix is really expensive to compute. Due to the sparse structure of the FIM, we always compute $\log(\det(\boldsymbol{C}))$ via $\log(\det(\boldsymbol{F}))$: $\log(\det(\boldsymbol{C})) \approx \log(\det(\boldsymbol{F}^{-1})) = -\log(\det(\boldsymbol{F}))$. Some references show that the D-optimality metric can keep monotonicity during the exploration [28]. Besides, the D-optimality metric and the entropy have an explicit relationship [29]. The D-optimality metric is a useful metric for quantifying the uncertainty of the estimated robot poses and the generated map in an active SLAM problem. In this part, we will derive the bounds of the D-optimality metric, which are easier to compute and can be used to approximate the original metric.

Some results about D-optimality design metric for the synchronization of the group $\mathbb{R}^2 \times SO(2)$ based on the block-isotropic Gaussian noise has been discussed in [6]. Because the situation using the isotropic Langevin noise on $\mathbb{R}^2 \times SO(2)$ is similar to the ones of [6], in this part, we only show the extended result for the group $\mathbb{R}^3 \times SO(3)$.

Theorem 3. *Considering the 3D pose-graph SLAM problem in Section III-B, its D-optimality design metric* $\log(\det(\boldsymbol{\mathcal{I}}_{3D}))$ *of the FIM has a lower bound* lb *and an upper bound* ub*:*

$$lb \le \log(\det(\boldsymbol{\mathcal{I}}_{3D})) \le ub, \tag{32}$$

where $lb = \log(\det(\boldsymbol{L}_w^{\mathbb{R}^3})) + \log(\det(\boldsymbol{L}_w^{SO(3)}))$, $ub = \log(\det(\boldsymbol{L}_w^{\mathbb{R}^3})) + \sum_{i=1}^{3n_p} \log(\lambda_i(\boldsymbol{L}_w^{SO(3)}) + \lambda_\infty)$, $\lambda_\infty = \|diag\{\boldsymbol{\Psi}_1, \cdots, \boldsymbol{\Psi}_{n_p}\}\|_{eig}$ *and* $\lambda_i(\boldsymbol{L}_w^{SO(3)})$ *means the* i*-th eigenvalue of* $\boldsymbol{L}_w^{SO(3)}$.

Proof: Based on the Schur's determinant formula [6] and (19), because $\boldsymbol{L}_w^{\mathbb{R}^3}$ is invertible, we have:

$$\begin{aligned} &\log(\det(\boldsymbol{\mathcal{I}}_{3D})) = \log(\det(\boldsymbol{L}_w^{\mathbb{R}^3})) + \log(\det(\boldsymbol{L}_w^{SO(3)} + \\ &\text{diag}\{\boldsymbol{\Psi}_1, \cdots, \boldsymbol{\Psi}_{n_p}\} - \triangle_w^{3D} \boldsymbol{L}_w^{\mathbb{R}^3 -1} \triangle_w^{3D\top})). \end{aligned} \tag{33}$$

Similar to the proof of Theorem 3 in [6], we can show $\triangle_w^{3D} \boldsymbol{L}_w^{\mathbb{R}^3 -1} \triangle_w^{3D\top} \succeq 0$ and $\text{diag}\{\boldsymbol{\Psi}_1, \cdots, \boldsymbol{\Psi}_{n_p}\} - \triangle_w^{3D} \boldsymbol{L}_w^{\mathbb{R}^3 -1} \triangle_w^{3D\top} \succeq 0$ are orthogonal projection matrices, then we have:

$$\begin{aligned} &lb = \log(\det(\boldsymbol{L}_w^{\mathbb{R}^3})) + \log(\det(\boldsymbol{L}_w^{SO(3)})) \le \\ &\log(\det(\boldsymbol{\mathcal{I}}_{3D})) \le \log(\det(\boldsymbol{L}_w^{\mathbb{R}^3})) + \log(\det(\boldsymbol{L}_w^{SO(3)} \\ &+ \text{diag}\{\boldsymbol{\Psi}_1, \cdots, \boldsymbol{\Psi}_{n_p}\})) < ub = \log(\det(\boldsymbol{L}_w^{\mathbb{R}^3})) \\ &+ \log(\det(\boldsymbol{L}_w^{SO(3)} + \lambda_\infty \boldsymbol{I}_{3n_p \times 3n_p})) \\ &= \log(\det(\boldsymbol{L}_w^{\mathbb{R}^3})) + \sum_{i=1}^{3n_p} \log(\lambda_i(\boldsymbol{L}_w^{SO(3)}) + \lambda_\infty). \end{aligned} \tag{34}$$

■

Some discussions about λ_∞ are shown as follows:

Corollary 1. *The biggest eigenvalue* λ_∞ *in Theorem 3 is smaller than* $\max_{i=1,2,\cdots,n_p} \frac{1}{2} \sum_{j\in V_i^+} \delta_{ij}^{-2} \|\boldsymbol{x}_j - \boldsymbol{x}_i\|_2^2$.

Proof: Based on the Rayleigh quotients [42] and Appendix F in supplementary material [40], we know that the variational description of the maximal eigenvalue $\lambda_\infty(\boldsymbol{\Psi}_i)$ of the real symmetric matrix $\boldsymbol{\Psi}_i,\ i = 1, \cdots, n_p$ is:

$$\begin{aligned} &\lambda_\infty(\boldsymbol{\Psi}_i) = \max_{\boldsymbol{x}\neq 0} \frac{\boldsymbol{x}^\top \boldsymbol{\Psi}_i \boldsymbol{x}}{\boldsymbol{x}^\top \boldsymbol{x}} = \\ &\max_{\boldsymbol{x}\neq 0} \frac{\boldsymbol{x}^T \sum_{j\in V_i^+} \boldsymbol{\Psi}_{(i,j)} \boldsymbol{x}}{\boldsymbol{x}^\top \boldsymbol{x}} \le \sum_{j\in V_i^+} \max_{\boldsymbol{x}\neq 0} \frac{\boldsymbol{x}^\top \boldsymbol{\Psi}_{(i,j)} \boldsymbol{x}}{\boldsymbol{x}^\top \boldsymbol{x}} \\ &= \sum_{j\in V_i^+} \lambda_\infty(\boldsymbol{\Psi}_{(i,j)}) = \sum_{j\in V_i^+} \frac{1}{2} \delta_{ij}^{-2} \|\boldsymbol{x}_j - \boldsymbol{x}_i\|_2^2. \end{aligned} \tag{35}$$

All eigenvalues of a block diagonal matrix are the eigenvalues of all block matrices on the diagonal [43], so we have:

$$\begin{aligned} \lambda_\infty &= \max_{i=1,2,\cdots,n_p} \lambda_\infty(\boldsymbol{\Psi}_i) \\ &\le \max_{i=1,2,\cdots,n_p} \frac{1}{2} \sum_{j\in V_i^+} \delta_{ij}^{-2} \|\boldsymbol{x}_j - \boldsymbol{x}_i\|_2^2. \end{aligned} \tag{36}$$

■

C. Discussion and comparison

1) Efficiency of the metric:

a) T-optimality metric: The parameters $w_{ij}^{SO(n)}$ and $w_{ij}^{\mathbb{R}}$ are constant. To simplify the discussion, we assume that these parameters are the same in every measurement for each pair of (i,j). Set: $c^{\omega} = dw_{ij}^{SO(n)} + nw_{ij}^{\mathbb{R}}$, based on (31), we have:

$$\text{trace}(\boldsymbol{\mathcal{I}}_{nD}) \approx \sum_{i=1}^{n_p} \sum_{j \in V_i} c^{\omega} = c^{\omega} \sum_{i=1}^{n_p} |V_i|, \ n = 2, 3, \quad (37)$$

where $\sum_{i=1}^{n_p} |V_i|$ means the total node degree of the graph.

Based on the approximation between the T-optimality metric and the node degree (37), we can get a simple conclusion: for fixed number of poses, minimizing the T-optimality metric is close to gathering as many measurements as possible. Moreover, we can also see the limitation of the T-optimality metric: when two graphs have the same total node degree and same node number, the T-optimality metric can not be used to distinguish their uncertainty levels. Two graphs in Figure 1 illustrate this.

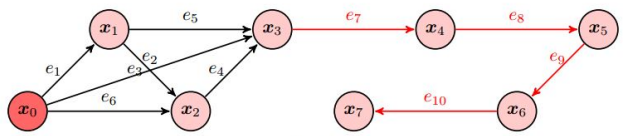

(a) $\mathcal{G}_1$ (pose-graph 1).

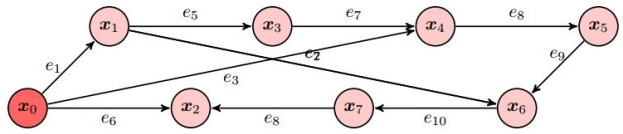

(b) $\mathcal{G}_2$ (pose-graph 2).

Fig. 1: Two examples of pose-graphs (with $\boldsymbol{x}_0$ as anchor)

Because of the same nodes and the same total node degree, graph 1 and graph 2 have the similar T-optimality objective function based on the equation (37). However, it is easy to know that graph 2 is much better than graph 1 because of the good loop closure. The uncertainty of poses $\boldsymbol{x}_4$ to $\boldsymbol{x}_7$ in graph 1 is larger than the ones in graph 2. So in some situations, the T-optimality metric is not very valuable.

b) D-optimality metric: For most pose-graph SLAM problems, the relative translations $\|\boldsymbol{x}_i - \boldsymbol{x}_j\|_2^2$ are usually small, so we have $ub \to lb$. Based on the bounds (34), we can get: $\log(\det(\boldsymbol{\mathcal{I}}_{nD})) \to lb = \log(\det(\boldsymbol{L}_w^{\mathbb{R}^n})) + \log(\det(\boldsymbol{L}_w^{SO(n)}))$. We can get the following theorem:

Theorem 4. *Considering the 2D/3D pose-graph SLAM problem in Section III-B,* $\xi \triangleq \max_{i=1,2,\cdots,n_p} \sum_{j \in V_i^+} \delta_{ij}^{-2} \|\boldsymbol{x}_j - \boldsymbol{x}_i\|_2^2$ *(2D) or* $\xi \triangleq \max_{i=1,2,\cdots,n_p} \frac{1}{2} \sum_{j \in V_i^+} \delta_{ij}^{-2} \|\boldsymbol{x}_j - \boldsymbol{x}_i\|_2^2$ *(3D) and* $\lambda_{min}(\boldsymbol{L}_w^{SO(n)})$ *is the minimal eigenvalue of* $\boldsymbol{L}_w^{SO(n)}$*, define* $\varepsilon = \log(\det(\boldsymbol{\mathcal{I}}_{nD})) - \log(\det(\boldsymbol{L}_w^{\mathbb{R}^n})) - \log(\det(\boldsymbol{L}_w^{SO(n)}))$*. Then we have,*

$$0 \leq \varepsilon \leq dn_p \log(1 + \xi / \lambda_{min}(\boldsymbol{L}_w^{SO(n)})). \quad (38)$$

Proof: Based on the equations (34) and (36), we have:

$$\begin{aligned} \varepsilon &= \log(\det(\boldsymbol{\mathcal{I}}_{nD})) - \log(\det(\boldsymbol{L}_w^{\mathbb{R}^n})) - \log(\det(\boldsymbol{L}_w^{SO(n)})) \\ &\leq \log(\det(\boldsymbol{L}_w^{SO(n)} + \xi \boldsymbol{I}_{dn_p \times dn_p})) - \log(\det(\boldsymbol{L}_w^{SO(n)})) \\ &= \log \prod_{i=1}^{dn_p} \frac{\lambda_i(\boldsymbol{L}_w^{SO(n)}) + \xi}{\lambda_i(\boldsymbol{L}_w^{SO(n)})} \leq \log \left(1 + \xi / \lambda_{min}(\boldsymbol{L}_w^{SO(n)})\right)^{dn_p} \\ &= dn_p \log \left(1 + \xi / \lambda_{min}(\boldsymbol{L}_w^{SO(n)})\right), \end{aligned} \quad (39)$$

where $\lambda_i(\boldsymbol{L}_w^{SO(n)})$, $i = 1, 2, \cdots, dn_p$ are the eigenvalues of $\boldsymbol{L}_w^{SO(n)}$, $\lambda_{min}(\boldsymbol{L}_w^{SO(n)})$ is the minimal eigenvalue of $\boldsymbol{L}_w^{SO(n)}$. ■

Based on Kirchhoff's matrix tree theorem [44], it is easy to know that $\det(\boldsymbol{L}_w^{\mathbb{R}^n})$ and $\det(\boldsymbol{L}_w^{SO(n)})$ are equivalent to the weighted number of spanning trees of the translation graph and the rotation graph. So, for a weighted graph $\mathcal{G}$ in pose-graph SLAM, the D-optimality design is almost equal to maximizing the weighted number of spanning trees of the graph $\mathcal{G}$ (also named weighted tree connectivity).

Remark 2. *The similar 2D pose-graph SLAM results with the Gaussian noise about the relationship between the D-optimality metric with the weighted tree connectivity have been discussed in [6]. In this paper, we extend it into the 3D pose-graph SLAM situation. Thus, results and all the further algorithms derived from these results (including* $k - ESP^+$ *problem [6]) can be extended to 3D case.*

2) Computational complexity:

a) T-optimality metric: After constructing the FIM, the computational complexity of the trace of the FIM is $O(n_p)$. In some special scenarios and applications, such as the active SLAM, some parts and some functions of the FIM can be reused in an incremental method. The complexity can be further reduced to $O(L_p)$, where L_p is the predicted horizon (MPC framework). It is easy to see that the T-optimality metric is a computational cost-effective metric.

b) D-optimality metric: We can see that the bounds lb and ub of the D-optimality metric of the FIM are almost independent of the values of the pose $\boldsymbol{x}_i$ and $\boldsymbol{R}_i$, which leads to robust performance. Beyond that, the update and operations on these bounds are easier than the real D-optimality metric of the FIM. In this part, we talk about the computational complexity of these bounds in 3D case (2D case is similar).

For the lower bound, we have two parts: $\log(\det(\boldsymbol{L}_w^{\mathbb{R}^3}))$ and $\log(\det(\boldsymbol{L}_w^{SO(3)}))$. Using the sparse Cholesky decomposition with a good fill-reducing permutation (Algorithm 1 in [6]), they can be computed much faster than the log-determinant function of the dense matrix $O(n_p^3)$; However, because $\boldsymbol{L}_w^{\mathbb{R}^3}$ and $\boldsymbol{L}_w^{SO(3)}$ have the same sparse structure, we can simply modify the original Algorithm 1 in [6] to a more efficient new algorithm (Algorithm 1).

In Algorithm 1, $(\star)_{i,i}$ means the i-th diagonal element of the matrix $\star$. The same order $\boldsymbol{l}$ in Algorithm 1 can also be used to compute the upper bound. This algorithm is similar to the Algorithm 1 in [6]. The only difference is to re-use the result of the column approximate minimum degree reordering algorithm because of the same sparse structure.

Algorithm 1 Lower bound computation for D-optimality metric (3D case)

1: **procedure** LB($\boldsymbol{L}_{w_{SO(3)}}, \boldsymbol{L}_{w_{\mathbb{R}}}$)
2: $\boldsymbol{l} \leftarrow COLAMD(\boldsymbol{L}_{w_{SO(3)}})$ ▷ Column approximate minimum degree permutation
3: $\boldsymbol{L}_1 \leftarrow SparseCholesky(\boldsymbol{L}_{w_{SO(3)}}(\boldsymbol{l},\boldsymbol{l}))$ ▷ Sparse Cholesky factor based on $\boldsymbol{l}$ for $\boldsymbol{L}_{w_{SO(3)}}$
4: $\boldsymbol{L}_2 \leftarrow SparseCholesky(\boldsymbol{L}_{w_{\mathbb{R}}}(\boldsymbol{l},\boldsymbol{l}))$ ▷ Sparse Cholesky factor based on the same $\boldsymbol{l}$ for $\boldsymbol{L}_{w_{\mathbb{R}}}$
5: **return** $6\sum_i (\log(\boldsymbol{L}_1)_{i,i} + \log(\boldsymbol{L}_2)_{i,i})$

For the upper bound ub, there are three parts: $\log(\det(\boldsymbol{L}_w^{\mathbb{R}^3}))$, $\lambda_i(\boldsymbol{L}_w^{SO(3)})$ and λ_∞. For $\lambda_i(\boldsymbol{L}_w^{SO(3)})$, we can use the Lanczos algorithm [45] and Fast Multi-pole Method [46] for the sparse Hermitian matrix (FIM is a sparse Hermitian matrix). The Lanczos algorithm can help to generate a tridiagonal real symmetric matrix from the matrix $\boldsymbol{L}_w^{SO(3)}$ in complexity $O(\bar{d}_n m_p n_p)$ or $O(\bar{d}_n n_p^2)$ if $m_p = n_p$ [47], where $\bar{d}_n$ is the average number of nonzero elements in a row of the matrix $\boldsymbol{L}_w^{SO(3)}$, m_p is the number of iterations in the Lanczos algorithm (as default, let $m_p = n_p$ [45]). For the generated tridiagonal matrices, the Fast Multi-pole Method computes all eigenvalues in just $O(n_p \log n_p)$ operations. So the computational complexity of $\lambda_i(\boldsymbol{L}_w^{SO(3)})$ is totally $O(\bar{d}_n n_p^2) + O(n_p \log n_p)$; For λ_∞, we have shown the analytical results $\lambda_\infty \approx \max_{i=1,2,\cdots,n_p} \frac{1}{2}\sum_{j\in V_i^+} \delta_{ij}^{-2}\|\boldsymbol{p}_{ij}\|_2^2$, which have the computational complexity $O(n_p)$.

The above discussion is based on the operations on the whole Laplacian matrix. Similar to the T-optimality metric, in some special scenarios and applications, such as the active SLAM, the incremental computation using the matrix determinant and re-use of calculation method (rAMDL) has been introduced into the computation of the D-optimality metric of the FIM [33]. Without the loop-closure, its computational complexity is reduced to $O(L_p^3)$, where L_p is usually constant and independent of the pose number n_p.

VIII. Experimental Results

In this section, we validate the correctness of our results and evaluate the performance of the bounds based on a variety of 2D/3D rigid body motion synchronization problems drawn from pose-graph SLAM. The datasets in this section are based on the open sources of the literature [3].

All experiments are performed on a HP EliteDesk 800 G2 desktop with an Intel Core i5-6500 3.20 GHz processor and 8 GB of RAM running Windows 10 Enterprise. Our experimental implementations are written in MATLAB R2016a.

A. Relation between optimality metrics with graph topology

In this experiment, we verify the results in Section VII-A3 and VII-C1a, which show that the T-optimality metric has a strong and direct relationship with the total node degree of the pose-graph as well as the D-optimality metric has a better performance in the uncertainty evaluation than the T-optimality metric. We use a small example with eight nodes to demonstrate this. A regular octagon is constructed based on these eight poses. The variances of the translation δ_{ij}^2 and the concentrations κ_{ij} of all measurements are set as 1×10^{-4} and 5×10^3, respectively. The initial pose graph only includes the odometer without the additional measurements, as shown in Fig. 2a. Then, we begin to add the measurements gradually from 1 edge to 21 edges without repetition. For example in Fig. 2b, we add 3 additional measurements. Then, for every graph, we can evaluate the trace and the log-determinant of the FIM after using SE-sync [3] to solve the SLAM problem. The optimality metric values (black points) and their corresponding total node degree (red line) are shown in Fig. 3 and 4. Each black point means the optimality metric corresponding to a pose-graph with the same 8 poses and unique additional measurements. For example, if the measurement number is 10, which means that we need to add 3 new measurements to the original graph shown in Fig. 2a and Fig. 2b. Based on combinatorics, we can generate all possible pose graphs with different measurements but the same poses, and then evaluate every pose graph using the optimality metric.

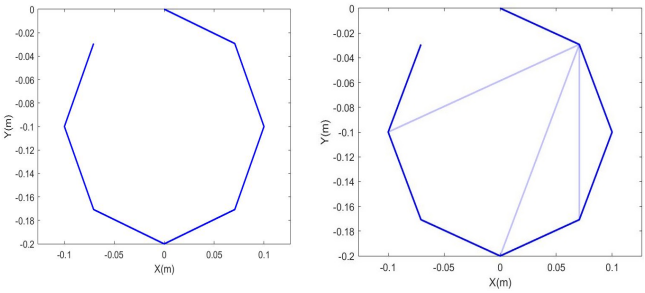

(a) Inital pose-graph (b) Pose-graph added 3 edges

Fig. 2: Pose-graph example

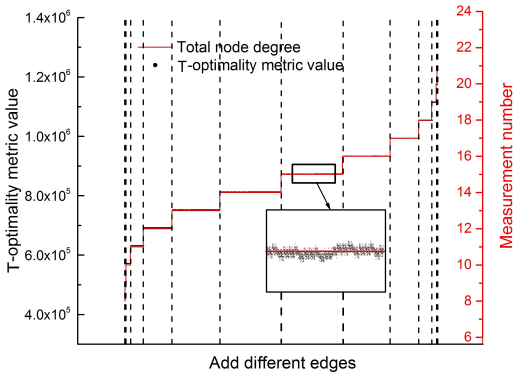

Fig. 3: Direct relationship between T-optimality metric with total node degree

In Fig. 3, we can find that the T-optimality metric is almost proportional to the total node degree of the whole pose graph, because the term $\sum_{i=1}^{n_p}\sum_{j\in V_i^+} \delta_{ij}^{-2}\|\boldsymbol{p}_{ij}\|_2^2$ is relatively small. The T-optimality metric values of the graphs, which have the same node degree, are similar. Directly using T-optimality metric may lead the obvious local minimal problem in its applications, such as the complex active SLAM problem. In Fig. 4, we can see that the D-optimality metric has a weaker connection with the total node degree compared with the T-optimality metric. We sort the D-optimality metric values of all possible graphs with $m = 12$ and $m = 13$ measurements. It can be seen that the D-optimality metric values with 13 measurements are smaller than the ones with 12 measurements

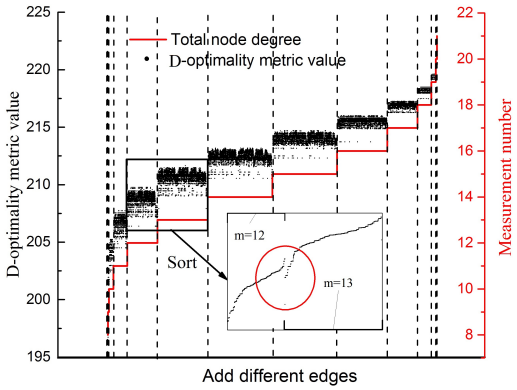

Fig. 4: Part relationship between D-optimality metric with total node degree

(pay attention to the red circle part). This situation is common for many real pose-graph SLAM problems. Even with fewer measurements, the SLAM problem with better network structure can have a better D-optimality metric, whose physical meaning is the volume of the covariance uncertainty.

B. T-/D-optimality metrics in active SLAM application

In this simulation, in order to further explore the applied efficiency of the T-/D-optimality metrics, we compare them in the active SLAM task, as shown in Fig. 5. Based on 100 random simulations with different designed way-points, we find that the optimal one selected by the T-optimality metric is commonly the same as the one picked out by the D-optimality metric (77%). Fig. 5 shows a result of which black and blue lines are respectively selected by the D-optimality metric and the T-optimality metric. The black path will lead more loops than the blue path, which leads to the smaller covariance value of the poses (black line: 1.2497×10^{-3} m, blue line: 1.2701×10^{-3} m). However, we also find that, when we pick out top 5 paths which have the big T-optimality metrics in every simulation as a set Ξ, the optimal one selected by the D-optimality metric will belong to Ξ with a very high probability (100%, 100 simulations). The above results show that these two metrics have a strong positive correlation, but still have some differences. The D-optimality metric is better than the T-optimality metric in the uncertainty evaluation.

Even though, sometimes, the T-optimality metric has the poorer performance than the D-optimality metric, it can be computed very fast. We can only use the diagonal elements of the FIM to compute the T-optimality metric. For the D-optimality metric, we need to construct the whole FIM and then compute the log-determinant function, which will obviously introduce the high computational complexity. It respectively costs 5.3934s and 0.4398s to compute the D-optimality metric and the T-optimality metric of 20 candidate paths with 170 poses and about 5206 measurements. The main advantage of the T-optimality metric is the better computational efficiency. So in our current work [49], we use the T-optimality metric or the weighted node degree to deal with the large-scale search for rough candidate actions, and the D-optimality or its lower bound (weighted tree connectivity) is applied for sophisticated search within a small elite group.

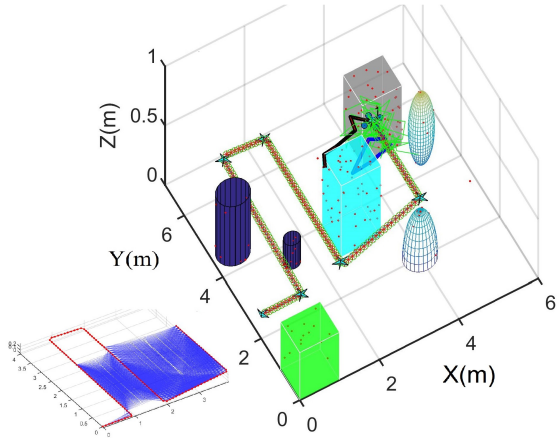

Fig. 5: Active SLAM task using two metrics. An unmanned aerial vehicle (UAV) moves from the first pentagram $(0, 2, 0.2)$, passes several pre-defined way-points (blue pentagrams), and meanwhile performs the SLAM task in the whole process. The green circles, the red stars, and the red points are respectively the real UAV trajectory, the estimated trajectory, and the detected features. The features will be detected when they locate in the sensor range of the UAV and we can get the relative pose measurements based on the common features between two poses. Using SE-sync, the obtained pose graph with the red nodes and the blue edges is shown in the small left-down figure. Finally, when it reaches $(4, 4.5, 0.5)$, the UAV aims to select the future paths by evaluating the T-/D-optimality metrics. 20 random candidate paths (green lines) with the same number of the additional poses are generated and evaluated. The optimal paths based on different metrics are selected. The black and blue lines are the paths respectively selected by the D-optimality and T-optimality metrics.

C. Bound efficiency on D-optimality metric

In this section, we evaluate the bound efficiency and computational advantage on a variety of classical heterogeneous pose-graph SLAM benchmarks. These datasets include: the synthetic datasets (3D: sphere, torus, and tiny/small/normal grid datasets) and the real-world datasets (2D: CSAIL, Intel Research Lab, manhattan (M3500), KITTI, city10000, and ais2klinik datasets; 3D: garage, cubicle, and rim datasets).

For the lower bound, the proposed Algorithm 1 is used to compute it. The largest eigenvalue of the weighted Laplacian matrix is obtained using the QR decomposition with the same ordering. Results for these experiments are shown in Table I (2D) and Table II (3D). We present the number of the poses and the measurements, the log-determinant of the FIM, its upper and lower bounds, and their computational time[5].

On each of these examples, the log-determinant of the FIM is bounded within lb and ub correctly. At the same time, lb and ub are very close to original metric in many datasets, especially for the lower bound lb. We can also find that, benefiting from the great dimensionality reduction, the computation of the upper and lower bounds of the log-determinant of the FIM is much cheaper than the ones of the original D-optimality metric. Because the dimension of the weighted Laplacian matrix is one-fourth (2D)/one-sixth (3D) of that of the full FIM, this great computational gap is sensible.

[5]It is noted that these results do not include the computational time of constructing process of the FIM and Laplacian matrix.

TABLE I: D-optimality metric results for the 2D pose-graph SLAM datasets

Dataset	# Poses	# Measurements	Original FIM		Upper bound		Lower bound	
			Metric value	Time $[s]$	Value	Time $[s]$	Value	Time $[s]$
CSAIL	1045	1172	1.9860×10^{4}	2.3284×10^{-3}	1.9876×10^{4}	9.2391×10^{-4}	1.9858×10^{4}	3.6712×10^{-4}
Intel	1728	2512	3.0194×10^{4}	6.0744×10^{-3}	3.0352×10^{4}	4.0055×10^{-3}	3.0155×10^{4}	2.0743×10^{-3}
manhattan	3500	5453	7.1124×10^{4}	3.3530×10^{-1}	7.1193×10^{4}	7.3602×10^{-3}	7.1104×10^{4}	4.5105×10^{-3}
KITTI	4541	4677	1.1697×10^{5}	8.9039×10^{-3}	1.1703×10^{5}	4.6468×10^{-3}	1.1695×10^{5}	3.1092×10^{-3}
city10000	10000	20687	1.6667×10^{5}	9.0052×10^{-2}	1.6816×10^{5}	2.4292×10^{-2}	1.6520×10^{5}	2.0664×10^{-2}
ais2klinik	15115	16727	2.3642×10^{5}	3.6301×10^{-2}	2.3975×10^{5}	1.4693×10^{-2}	2.3567×10^{5}	1.3116×10^{-2}

TABLE II: D-optimality metric results for the 3D pose-graph SLAM datasets

Dataset	# Poses	# Measurements	Original FIM		Upper bound		Lower bound	
			Metric value	Time $[s]$	Value	Time $[s]$	Value	Time $[s]$
tiny-grid	9	11	2.4562×10^{2}	2.1558×10^{-4}	2.7561×10^{2}	2.9866×10^{-2}	2.4163×10^{2}	1.4115×10^{-4}
small-grid	125	297	4.4452×10^{3}	3.6373×10^{-3}	4.8488×10^{3}	3.1836×10^{-2}	4.3815×10^{3}	4.3020×10^{-4}
garage	1661	6275	2.0618×10^{4}	3.9511×10^{-2}	3.6618×10^{4}	3.6117×10^{-2}	1.5845×10^{4}	2.2989×10^{-3}
sphere	2500	4949	9.9105×10^{4}	7.4856×10^{-2}	1.0607×10^{5}	7.4023×10^{-2}	9.9054×10^{4}	6.7317×10^{-3}
torus	5000	9048	2.4986×10^{5}	1.9488×10^{-1}	2.6526×10^{5}	1.0156×10^{-1}	2.4985×10^{5}	1.6390×10^{-2}
cubicle	5750	16869	2.3729×10^{5}	2.1579×10^{-1}	3.1839×10^{5}	5.2156×10^{-2}	2.3685×10^{5}	1.4141×10^{-2}
grid	8000	22236	4.2613×10^{5}	3.2318×10^{0}	4.4902×10^{5}	1.5065×10^{-1}	4.2610×10^{5}	9.0280×10^{-2}
rim	10195	29743	4.7257×10^{5}	4.1626×10^{-1}	5.8622×10^{5}	6.5298×10^{-2}	4.7209×10^{5}	4.1260×10^{-2}

It is easy to find that, except the 'garage' dataset[6], the log-determinant of the whole FIM gets closed to its lower bound (in 103%), because of the small term $\sum_{i=1}^{n_p}\sum_{j\in V_i^+}\delta_{ij}^{-2}\|\boldsymbol{p}_{ij}\|_2^2$. So in the real applications of the D-optimality metric, such as the active pose-graph SLAM [48], we suggest using the tight lower bound, whose physical meaning is the sum of the weighted number of the spanning trees of two graphs, to replace the original objective function.

Besides the computational time of obtaining these metrics, we also show the computational time of constructing the whole FIM, the weighted Laplacian matrix for $\mathbb{R}^2$ and $\mathbb{R}^3$ parts and the weighted Laplacian matrix for $SO(2)$ and $SO(3)$ parts. They are used to compute the metrics. Table III and Table IV show the computational time. The results show that the sparser weighted Laplacian matrices for the lower bound are much easier to be constructed than the whole FIM.

TABLE III: Matrix constructing time for the 2D SLAM datasets

Dataset	Time $[s]$	
	Whole FIM	Weighted Laplacian matrices
CSAIL	8.8581×10^{-2}	1.5723×10^{-2}
Intel	1.3518×10^{-1}	1.9283×10^{-2}
manhattan	2.3982×10^{-1}	2.6794×10^{-2}
KITTI	2.2071×10^{-1}	2.5118×10^{-2}
city10000	7.3709×10^{-1}	6.3875×10^{-2}
ais2klinik	6.3033×10^{-1}	5.4222×10^{-2}

TABLE IV: Matrix constructing time for the 3D SLAM datasets

Dataset	Time $[s]$	
	Whole FIM	Weighted Laplacian matrices
tiny-grid	7.1865×10^{-2}	2.0968×10^{-2}
small-grid	1.1677×10^{-1}	1.9557×10^{-2}
garage	9.6897×10^{-1}	5.3639×10^{-2}
sphere	8.3076×10^{-1}	4.8680×10^{-2}
torus	1.3884×10^{0}	7.3766×10^{-2}
cubicle	2.3300×10^{0}	1.1033×10^{-1}
grid	3.0566×10^{0}	1.1413×10^{-1}
rim	4.0647×10^{0}	1.7824×10^{-1}

D. Efficiency of CRLB

In this section, our main purpose is to validate that the CRLB is reachable using SE-sync method (which belongs to maximum likelihood estimator) [3]. These experiments are based on 'tiny-3Dgrid' and 'CSAIL' datasets.

In order to compute the covariance by the statistical way, we need a ground truth and then sample noises to it. The ground truth is obtained by the optimization results of original datasets presented in [3] using SE-sync. Then, we set these estimated poses as the ground truth. After obtaining the ground truth, the random noises obeying the isotropic Gaussian distribution and the isotropic Lagevin distribution are generated. We use 'normrnd' MATLAB function to generate the isotropic Gaussian distribution. For the isotropic Lagevin distribution, the noises are generated by the Acceptance-Rejection Method (ARM) [50]. Then we can add these noises into our relative measurements by the edge data using following equations:

$$\begin{aligned}\boldsymbol{H}_{ij} &= \boldsymbol{Z}_{ij}\boldsymbol{R}_j\boldsymbol{R}_i^{\top}, \boldsymbol{Z}_{ij}\sim Lang(\boldsymbol{I}_{n\times n}, k_c\cdot\kappa_{ij})\\ \boldsymbol{p}_{ij} &= \boldsymbol{R}_i^{\top}(\boldsymbol{x}_j-\boldsymbol{x}_i)+\boldsymbol{y}_{ij}, \boldsymbol{y}_{ij}\sim\mathcal{N}(\boldsymbol{0}, \delta_{ij}^2\boldsymbol{I}_{n\times n}),\end{aligned} \tag{40}$$

where k_c is the coefficient to determine the uncertainty level of the rotation measurement. $k_c\cdot\kappa_{ij}$ is the concentration of the noise[7].

[6]The 'garage' dataset has a poor measurement network, whose weighted values of measurement edges are small (large covariance), and the translation values between different poses are large. Both of these two properties make that the term $\sum_{i=1}^{n_p}\sum_{j\in V_i^+}\delta_{ij}^{-2}\|\boldsymbol{x}_j-\boldsymbol{x}_i\|_2^2$ is relatively large compared with the term $\log(\det(\boldsymbol{L}_w^{\mathbb{R}^n}))+\log(\det(\boldsymbol{L}_w^{SO(n)}))$. This situation is not very common in the real world datasets.

[7]It is noted that we only consider the uncertainty level of the rotation measurement in our SNR definition (22).

For the estimated results, the trace of covariance is:

$$\text{trace}(\boldsymbol{C}) = \mathbb{E}\{\sum_{i=1}^{n_p} \left(\text{dist}(\boldsymbol{R}_i, \bar{\boldsymbol{R}}_i)^2 + \|\boldsymbol{x}_i - \bar{\boldsymbol{x}}_i\|_2^2\right)\}, \quad (41)$$

where $\bar{\star}$ means the ground truth of $\star$. Every measurement dataset can generate a value using (41), then repeat many times to obtain the mathematical expectation $\mathbb{E}\{\text{trace}(\boldsymbol{C})\}$ by average. Finally, we can compute and compare the CRLB and the average mean squared error (MSE) for every pose.

For the 2D situation, we use the 'CSAIL' dataset to obtain the average MSE and CRLB. The initial κ_{ij} and δ_{ij}^{-2} are respectively set as 150 and 140. The coefficient k_c changes from 1 to 20. The simulations are repeated 100 times to get the covariance matrix. The results are shown in Fig. 6.

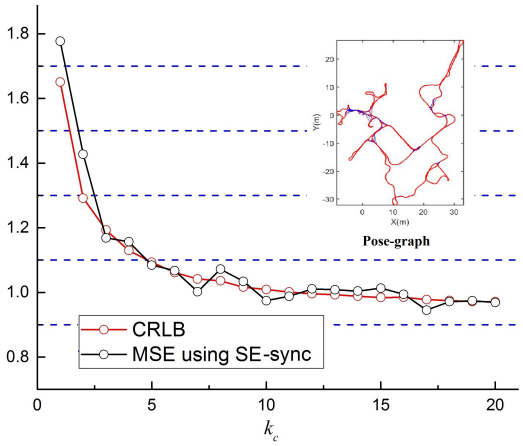

Fig. 6: Comparison of the CRLB with the mean squared error ($MSE = \frac{\text{trace}(\boldsymbol{C})}{n_p}$) of known estimators for the synchronization of $n_p = 1045$ poses with $m = 1172$ measurements and one anchor based on the 'CSAIL' dataset. The MSE using the SE-sync method appears to reach the CRLB.

For the 3D situation, we use the 'tiny-3Dgrid' dataset to obtain the covariance, CRLB with curvature terms and CRLB without curvature terms. κ_{ij} is set as 12.5 and the coefficient k_c changes from 1 to 20. Based on the Monte Carlo simulation, the processes are repeated 50 times. The simulation results are shown in Fig. 7.

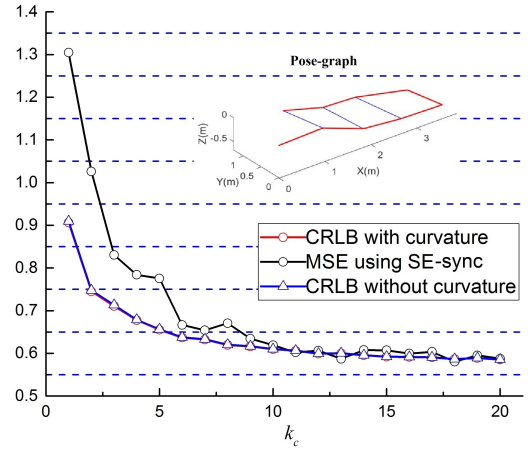

Fig. 7: Comparison of the CRLB with the mean squared error ($MSE = \frac{\text{trace}(\boldsymbol{C})}{n_p}$) of known estimators for the synchronization of $n_p = 9$ poses with $m = 11$ measurements and one anchor based on the 'tiny-3Dgrid' dataset. The MSE using the SE-sync method appears to reach the CRLB.

The above two simulations show two key points. The first one is that the CRLB is reachable when the SNR is large enough. The other one is that, compared with the $\boldsymbol{F}^{-1}$, the curvature tensor of the parameter space $\mathcal{P}_3$ is negligible.

IX. Conclusion, Potential Applications and Future Work

Based on the assumption of the isotropic Langevin noise for rotation and the block-isotropic Gaussian noise for translation, the FIM and CRLB of 2D/3D pose-graph SLAM, which are formulated as the synchronization on $\mathbb{R}^n \times SO(n),\ n = 2, 3$, are derived and shown to be closely related to the weighted Laplacian matrix of pose-graph SLAM. Then, the TOED metrics, including T-optimality and D-optimality, are discussed. It shows that the T-optimality metric is almost directly determined by the total node degree, and the D-optimality design is almost equivalent to maximizing the weighted tree-connectivity. We find that the T-optimality metric is cheaper than the D-optimality metric, but the D-optimality metric has a better performance in terms of the uncertainty evaluation. Furthermore, the lower and upper bounds of the D-optimality metric are presented, which are cheaper and can be used to approximate the original metric. The experiment results, which verify our standpoints, are performed based on both the synthetic datasets and the real-world datasets.

There are multiple kinds of potential applications using our obtained results. Two examples of the applications are active SLAM and measurement selection.

Active SLAM is a decision making problem where the robot's trajectory is chosen both to improve the SLAM results, and meanwhile, to perform other tasks such as coverage or exploration [51]. The optimal design metrics of the FIM and the covariance matrix are the most common objective function in active SLAM [52] and other belief space planning problems [33]. The computation complexity of the objective function is one of the key issues in active SLAM. This paper presents the new metrics, including weighted node degree and weighted tree connectivity, in 2D/3D situation for active SLAM, which helps to improve the real-time ability [51]. In future, we will apply these metrics to perform the on-line active SLAM using some plat-forms, like quad-rotor UAV and other robots.

Because of the limitation of the weight, size, power budgets, and on-board hardware capability of the robot, for the scalable and long-term autonomy, the measurement selection is one of several mechanisms through which the SLAM systems can achieve resource adaptation. In [6], based on the 2D result, the measurement selection problem, which is proved to be a sub-modular optimization problem, is solved by the greedy algorithm and the convex relaxation method. This edge selection problem shows its enormous potential applications in the front/back-end computational reduction [6] and resource assignment in cooperative SLAM [53].

The results presented in this paper are only the first step towards the use of graph topology in areas such as active SLAM, measurement selection, anchor selection, and so on. Similar to our work [51], we are trying to use these technologies into the planning and decision making pipelines. The further study on the FIM, CRLB and optimal design metric for $SE(3)$ (special Euclidean) group will be another interesting research direction.

ACKNOWLEDGMENT

We would like to thank A. Prof. N. Boumal, who has answered many of our queries about his research [1] and [12], which helps us significantly in this work. We want to thank Dr. David M. Rosen for sharing us the code to generate the random noise for our simulation. We would like to thank Dr. K. Khosoussi, Dr. E. Zhang, Dr. D. Li, A. Prof. J. Chu, Mr. F. Bai, and Dr. J. Wang for the many productive conversations and input over the course of this work. Finally, we would like to thank the anonymous reviewers for their constructive feedback, which improves the overall quality of the paper.

REFERENCES

[1] N. Boumal, "On intrisic Cramér-Rao bounds for Riemannian submanifolds and quotient manifolds," *IEEE Trans. Signal Process*, vol. 61, no. 7, pp. 1809-1821, Jan. 2013.

[2] C. Cadena, L. Carlone, H. Carrillo, Y. Latif, D. Scaramuzza, J. Neira, I. Reid, and J. J. Leonard, "Past, present, and future of simultaneous localization and mapping: toward the robust-perception age," *IEEE Trans. on Robot.*, vol. 32, no. 6, pp. 1309-1332, Dec. 2016.

[3] D. M. Rosen, L. Carlone, A. S. Bandeira, and J. J. Leonard, "SE-Sync: A certifiably correct algorithm for synchronization over the special Euclidean group," *Int. J. Robot. Res.*, vol. 38, no. 2-3, pp. 95-125, Mar. 2018.

[4] J. Briales and J. G. Jimenez, "Cartan-Sync: Fast and global SE(d)-synchronization," *IEEE Robot. and Autom. Lett.*, vol. 2, no. 4, pp. 2127-2134, Jun. 2017.

[5] K. Khosoussi, S. Huang, and G. Dissanayake, "Tree-connectivity: evaluating the graphical structure of SLAM," in *Proc. IEEE Int. Conf. Robot. Autom.*, May 2016, pp. 1316-1322.

[6] K. Khosoussi, M. Giamou, G. S. Sukhatme, S. Huang, G. Dissanayake, and J. P. How, "Reliable graph for SLAM," *Int. J. Robot. Res.*, vol. 38, no. 2-3, pp. 260-298, Jan. 2019.

[7] H. Cramér, (1946). Mathematical methods of statistics. Princeton, NJ: Princeton Univ. Press.

[8] S. Wenhardt, B. Deutsch, E. Angelopoulou, and H. Niemann, "Active visual object reconstruction using D-, E-, and T-optimal next best views," in *Proc. IEEE Conf. Comp. Vision and Patt. Recogn.*, Jun. 2007, pp. 1-7.

[9] X. Shen and P. K. Varshney, "Sensor selection based on generalized information gain for target tracking in large sensor networks," *IEEE Trans. on Signal Processing*, vol. 62, no. 2, pp. 363-375, Nov. 2014.

[10] S. Liu, S. P. Chepuri, M. Fardad, G. Leus, and P. K. Varshney, "Sensor selection for estimation with correlated measurement noise," *IEEE Trans. on Signal Processing*, vol. 64, no. 13, pp. 3509-3522, Apr. 2016.

[11] R. A. Bailey and P. J. Cameron, "Combinatorics of optimal designs," *Surveys in Combinatorics*, vol. 365, pp. 19-73, 2009.

[12] N. Boumal, A. Singer, P. A. Absil, and V. D. Blondel, "Cramér-Rao bounds for synchronization of rotations," *Information and Inference: A J. of the IMA*, vol. 3, no. 1, pp. 1-39, Mar. 2013.

[13] R. Kmmerle, G. Grisetti, H. Strasdat, K. Konolige, and W. Burgard. "G2o: A general framework for graph optimization," in *Proc. IEEE Int. Conf. Robot. Autom.*, May 2011, pp. 3607-3613.

[14] M. Kaess, H. Johannsson, R. Roberts, V. Ila, J. J. Leonard, and F. Dellaert. "iSAM2: Incremental smoothing and mapping using the Bayes tree," *Int. J. Robot. Res.*, vol. 31, no. 2, pp. 216-235, Feb. 2012.

[15] V. Ila, L. Polok, M. Solony, and P. Svoboda. "SLAM++-A highly efficient and temporally scalable incremental SLAM framework," *Int. J. Robot. Res.*, vol. 36, no. 2, pp. 210-230, Feb. 2017.

[16] S. Agarwal and K. Mierle, Ceres Solver, http://ceres-solver.org.

[17] L. Carlone, G. C. Calafiore, C. Tommolillo, and F. Dellaert. "Planar pose graph optimization: Duality, optimal solutions, and verification," *IEEE Trans. on Robot.*, vol. 32, no. 3, pp. 545-565, May 2016.

[18] O. Ozyesil, N. Sharon, and A. Singer. "Synchronization over Cartan motion groups via contraction," *SIAM J. on Applied Algebra and Geometry*, vol. 2, no. 2, pp. 207-241, Apr. 2018.

[19] L. Carlone, and G. C. Calafiore. "Convex relaxations for pose graph optimization with outliers," *IEEE Robot. and Autom. Lett.*, vol. 3, no. 2, pp. 1160-1167, Jan. 2018.

[20] J. Briales and J. G. Jimenez, "Convex global 3D registration with Lagrangian duality," in *Proc. IEEE Conf. Comp. Vision and Patt. Recogn.*, Jul. 2017, pp. 4960-4969.

[21] O. Ozyesil and A. Singer, "Robust camera location estimation by convex programming," in *Proc. IEEE Conf. Comp. Vision and Patt. Recogn.*, Jun. 2015, pp. 2674-2683.

[22] R. C. Rao, "Information and accuracy attainable in the estimation of statistical parameters," *Breakthroughs in stat.*, vol. 37, pp. 81-91, 1945.

[23] S. Smith, "Covariance, subspace, and intrinsic Cramér-Rao bounds," *IEEE Trans. Signal Process*, vol. 53, no. 5, pp. 1610-1630, 2005.

[24] J. Xavier and V. Barroso, "Intrinsic variance lower bound: an extension of the Cramr-Rao bound to Riemannian manifolds," in *IEEE Int. Conf. Acoustics, Speech, and Signal Processing*, May 2005, pp. 1033-1036.

[25] P. Vakili, H. Mirzaei, S. Zarbafian, I. C. Paschalidis, D. Kozakov, and S. Vajda, "Optimization on the space of rigid and flexible motions: an alternative manifold optimization approach," in *Proc. IEEE Annual Conf. on Decision and Control*, Dec. 2014, pp. 5825-5830.

[26] O. Brüls, M. Arnold, and A. Cardona, "Two Lie group formulations for dynamic multibody systems with large rotations," in *Proc. ASME Int. Design Eng. Technical Conf.*, Jan. 2011, pp. 85-94.

[27] L. Carlone, R. Tron, K. Daniilidis, and F. Dellaert, "Initialization techniques for 3D SLAM: a survey on rotation estimation and its use in pose graph optimization," in *Proc. IEEE Int. Conf. Robot. Autom.*, May 2015, pp. 4597-4604.

[28] H. Carrillo, Y. Latif, M. L. Rodrguez, and J. A. Castellanos, "On the monotonicity of optimality criteria during exploration in active SLAM," in *Proc. IEEE Int. Conf. Robot. Autom.*, May 2015, pp. 1476-1483.

[29] H. Carrillo, I. Reid, and J. A. Castellanos, "On the comparison of uncertainty criteria for active SLAM," in *Proc. IEEE Int. Conf. Robot. Autom.*, May 2012, pp. 2080-2087.

[30] Y. Kim and A. Kim, "On the uncertainty propagation: Why uncertainty on Lie groups preserves monotonicity?" in *Proc. IEEE/RSJ Int. Conf. Intell. Robots Syst.*, Sep. 2017, pp. 3425-3432.

[31] M. L. Rodríguez-Arévalo, J. Néira, and J. A. Castellanos. "On the importance of uncertainty representation in active SLAM," *IEEE Trans. on Robot.*, vol. 34, no. 3, pp. 829-834, Apr. 2018.

[32] T. D. Barfoot and P. T. Furgale. "Associating uncertainty with three-dimensional poses for use in estimation problems," *IEEE Trans. on Robot.*, vol. 30, no.3, pp. 679-693, Jan. 2014.

[33] D. Kopitkov and V. Indelman, "No belief propagation required: Belief space planning in high-dimensional state spaces via factor graphs, the matrix determinant lemma, and re-use of calculation," *Int. J. Robot. Res.*, vol. 36, no. 10, pp. 1088-1130, Sep. 2017.

[34] K. Khosoussi, S. Huang, and G. Dissanayake, "Novel insights into the impact of graph structure on SLAM," in *Proc. IEEE/RSJ Int. Conf. Intell. Robots Syst.*, Sep. 2014, pp. 2707-2714.

[35] Wolfram, (2001), Modified Bessel function of the first kind: Integral representations. http://functions.wolfram.com/03.02.07.0007.01.

[36] J.C. Simo and L. Vu-Quoc, "On the dynamics in space of rods undergoing large motionsa geometrically exact approach," *Comput. Methods in Appl. Mech. and Eng.*, vol. 66, no. 2, pp. 125-161, Feb. 1988.

[37] P. A. Absil, R. Mahony, and R. Sepulchre, (2008) Optimization algorithms on matrix manifolds. Princeton, NJ: Princeton University Press.

[38] T. D. Barfoot, (2017). State estimation for robotics, Cambridge University Press.

[39] E. Eade, (2011). Lie groups for 2d and 3d transformations, http://ethaneade.com/lie.pdf, revised May. 2017.

[40] Y. Chen, L. Zhao, S. Huang, and G. Dissanayake, Cramér-Rao bounds and optimal design metrics for pose-graph SLAM, (Supplementary Material), IEEE transactions on Robotics, 2020.

[41] M. P. Do Carmo (1992). Riemannian geometry. Birkhauser.

[42] J. R. Magnus and H. Neudecker, (1988). Matrix differential calculus with applications in statistics and econometrics. Wiley series in probability and mathematical statistics.

[43] D. A. Harville, (1997). Matrix algebra from a statistician's perspective, Springer.

[44] S. Chaiken and D. J. Kleitman. "Matrix tree theorems," *J. of combinatorial theory*, Series A, vol. 24, no. 3, pp. 377-381, May 1978.

[45] C. Lanczos, "An iteration method for the solution of the eigenvalue problem of linear differential and integral operators," *J. of Res. of the National Bureau of Standards*, vol. 45, no. 4, pp. 255-282, Oct. 1950.

[46] E. S. Coakley and V. Rokhlin. "A fast divide-and-conquer algorithm for computing the spectra of real symmetric tridiagonal matrices," *Appl. and Comput. Harmon. Analysis*, vol. 34, no. 3, pp. 379-414, May 2013.

[47] Y. Saad. "Numerical methods for large eigenvalue problems: revised edition," *Siam*, 2011.

[48] R. Valencia, M. Morta, J. Andrade-Cetto, and J. M. Porta. "Planning reliable paths with pose SLAM," *IEEE Trans. on Robot.*, vol. 29, no. 4, pp. 1050-1059, Apr. 2013.

[49] Y. Chen, S. Huang, R. Fitch, L. Zhao, and D. Yang. "On-line 3D active pose-graph SLAM based on key poses using graph topology and submaps," in *Proc. IEEE Int. Conf. Robot. Autom.*, May 2019, pp. 169-175.
[50] B. D. Flury. "Acceptance-rejection sampling made easy," *SIAM Review*, vol. 32, no.3, pp. 474-476, Sep. 1990.
[51] Y. Chen, S. Huang, and R. Fitch, "Active SLAM for Mobile Robots with Area Coverage and Obstacle Avoidance," *IEEE-ASME Trans. on Mech.*, Jan. 2020.
[52] S. Huang, N. M. Kwok, G. Dissanayake, and Q. P. Ha, "Multi-step look-ahead trajectory planning in SLAM: Possibility and necessity," in *Proc. IEEE Int. Conf. Robot. Autom.*, May 2005, pp. 1091-1096.
[53] M. Giamou, K. Khosoussi, and J. P. How, "Talk resource-efficiently to me: Optimal communication planning for distributed loop closure detection," in *Proc. IEEE Int. Conf. Robot. Autom.*, May 2018, pp. 3841-3848.

Yongbo Chen received the bachelors in engineering from Beijing Institute of Technology (BIT), Beijing, China, in 2012. He is now a PhD candidate with the Centre for Autonomous Systems, Faculty of Engineering and Information Technology, University of Technology Sydney, Sydney, Australia. His research interests include UAV motion/mission planning, mobile robots simultaneous localization and mapping (SLAM), and non-rigid structure from motion (NRSfM).

Shoudong Huang received the Ph.D. degree in automatic control from Northeastern University, Shenyang, China, in 1998. He is currently an Associate Professor with the Centre for Autonomous Systems, Faculty of Engineering and Information Technology, University of Technology Sydney, Sydney, Australia. His research interests include mobile robots simultaneous localization and mapping (SLAM), robot path planning and control.

Liang Zhao received the PhD degree in photogrammetry and remote sensing from Peking University, Beijing, China, in 2013. From 2014-2016, he worked as a Postdoctoral Research Associate in the Hamlyn Centre for Robotic Surgery, Department of Computing, Faculty of Engineering, Imperial College London, United Kingdom. He is a Senior Lecturer in CAS, UTS since July 2016. His current research interests include surgical robotics, SLAM, Structure-from-Motion, and aerial photogrammetry.

Gamini Dissanayake graduated in mechanical/production engineering from University of Peradeniya, Peradeniya, Sri Lanka, and received the B.Sc. (Eng), M.Sc. degree in machine tool technology and the Ph.D. degree in mechanical engineering from University of Birmingham, Birmingham, U.K., in 1981 and 1985, respectively. He is the James N Kirby Distinguished Professor of mechanical and mechatronic engineering with University of Technology Sydney, Sydney, Australia. His research interests include localization and map building for mobile robots, navigation systems, dynamics, and control of mechanical systems, cargo handling, optimization, and path planning.